Architecture of an embracing lipase-foldase complex of the type II secretion system of Acinetobacter baumannii

Yuri Rafael de Oliveira Silva, Carlos Contreras-Martel, Ricardo Rodrigues de Melo, Letícia Maria Zanphorlin, Daniel Maragno Trindade, Andréa Dessen

▶ **To cite this version:**

Yuri Rafael de Oliveira Silva, Carlos Contreras-Martel, Ricardo Rodrigues de Melo, Letícia Maria Zanphorlin, Daniel Maragno Trindade, et al.. Architecture of an embracing lipase-foldase complex of the type II secretion system of Acinetobacter baumannii. Structure, 2025, 33 (3), pp.601-612.e4. ⟨10.1016/j.str.2024.12.022⟩. ⟨hal-04981231⟩

HAL Id: hal-04981231

https://hal.science/hal-04981231v1

Submitted on 24 Nov 2025

HAL is a multi-disciplinary open access archive for the deposit and dissemination of scientific research documents, whether they are published or not. The documents may come from teaching and research institutions in France or abroad, or from public or private research centers.

L'archive ouverte pluridisciplinaire **HAL**, est destinée au dépôt et à la diffusion de documents scientifiques de niveau recherche, publiés ou non, émanant des établissements d'enseignement et de recherche français ou étrangers, des laboratoires publics ou privés.

HAL Authorization

Structure

Article

Architecture of an embracing lipase-foldase complex of the type II secretion system of *Acinetobacter baumannii*

Graphical abstract

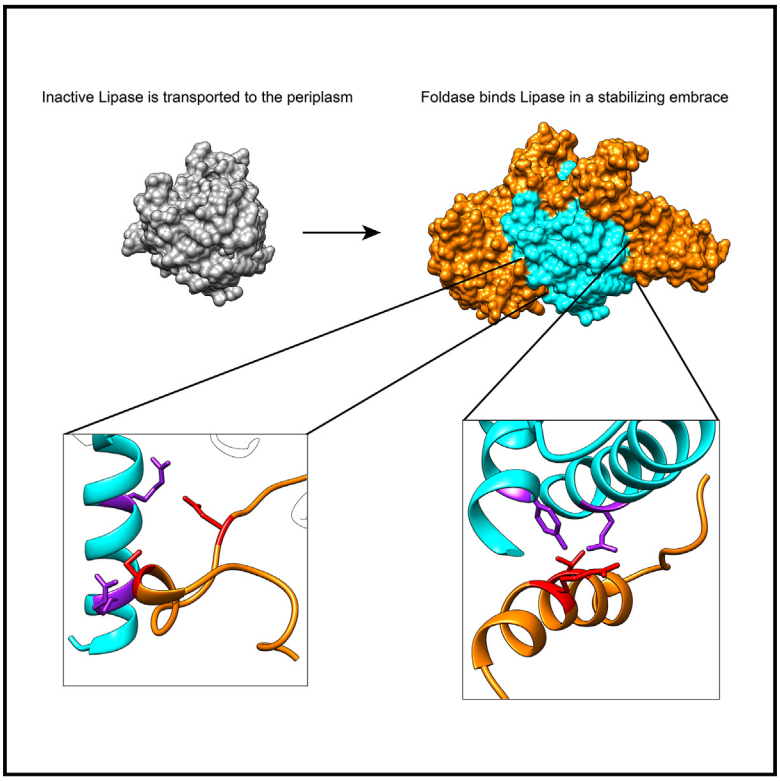

Highlights

- Lipase-specific foldases are widespread in Proteobacteria
- T2SS-secreted virulence factor LipA is active while bound to the foldase LipB
- The structure of the LipA-LipB complex reveals an unusual, extended interface area
- Four highly conserved interacting residues may be essential for LipB function

Authors

Yuri Rafael de Oliveira Silva, Carlos Contreras-Martel, Ricardo Rodrigues de Melo, Letícia Maria Zanphorlin, Daniel Maragno Trindade, Andréa Dessen

Correspondence

daniel.trindade@lnbio.cnpem.br (D.M.T.), andrea.dessen@cnrs.fr (A.D.)

In brief

De Oliveira Silva et al. characterized the unusual structure of a complex between a lipase secreted by the pathogen *Acinetobacter baumannii* and its chaperone. Bioinformatic analyses show that this chaperone family is more diverse than previously thought, and key conserved residues involved in interactions between the two proteins are highlighted.

de Oliveira Silva et al., 2025, Structure *33*, 1–12
March 6, 2025 © 2025 Elsevier Inc. All rights reserved, including those for text and data mining, AI training, and similar technologies.
https://doi.org/10.1016/j.str.2024.12.022

CellPress

Please cite this article in press as: de Oliveira Silva et al., Architecture of an embracing lipase-foldase complex of the type II secretion system of *Acinetobacter baumannii*, Structure (2025), https://doi.org/10.1016/j.str.2024.12.022

Structure

CellPress

Article

Architecture of an embracing lipase-foldase complex of the type II secretion system of *Acinetobacter baumannii*

Yuri Rafael de Oliveira Silva,[1,2] Carlos Contreras-Martel,[3] Ricardo Rodrigues de Melo,[4] Letícia Maria Zanphorlin,[4] Daniel Maragno Trindade,[1,*] and Andréa Dessen[3,5,*]

[1]Brazilian Biosciences National Laboratory (LNBio), CNPEM, Campinas São Paulo 13084-971, Brazil
[2]Departamento de Genética, Evolução, Microbiologia e Imunologia, Instituto de Biologia, Universidade Estadual de Campinas (UNICAMP), Campinas, São Paulo 13083-970, Brazil
[3]University Grenoble Alpes, CNRS, CEA, Institut de Biologie Structurale (IBS), 38044 Grenoble, France
[4]Brazilian Biorenewables National Laboratory (LNBR), CNPEM, Campinas São Paulo 13084-971, Brazil
[5]Lead contact
*Correspondence: daniel.trindade@lnbio.cnpem.br (D.M.T.), andrea.dessen@cnrs.fr (A.D.)
https://doi.org/10.1016/j.str.2024.12.022

SUMMARY

Acinetobacter baumannii is a major human pathogen responsible for a growing number of multi-antibiotic-resistant infections, and of critical priority for the World Health Organization (WHO). *A. baumannii* employs a type II secretion system (T2SS) to secrete toxins extracellularly to enable cytotoxicity and colonization. Lipase LipA, secreted by the *A. baumannii* T2SS, is required for virulence and fitness, and in the periplasm is maintained in an active state by its essential foldase, LipB. Here we report that LipA is able to recognize lipids of different chain lengths at extremes of pH and temperature, thanks to its stabilization by LipB through an extended, highly helical "embrace." A vast bioinformatic analysis indicates that LipB-like foldases are widespread over numerous proteobacteria, and thus the extended foldase architecture shown here could be widespread. These results provide new insight into *A. baumannii*'s adaptability as a pathogen in different environments and could facilitate the development of novel antibacterials.

INTRODUCTION

Acinetobacter baumannii is an opportunistic human pathogen that in the last few years has presented multi-drug resistance (MDR) rates that can be up to four times higher than those observed for other major Gram-negative pathogens.[1] *A. baumannii* is a global threat in community and health care settings, where it can resist prolonged periods of desiccation as well as disinfection procedures.[2] *A. baumannii* can form robust biofilms, hampering treatment with different antibiotics,[3] and the World Health Organization (WHO) has included carbapenem-resistant *A. baumannii* in the list of pathogens for which novel treatments are most urgently needed.

Several virulence factors have been shown to play roles both in *A. baumannii*'s pathogenesis and its ability to generate biofilms. This includes phospholipases, porins, and two-component efflux pumps; capsular polysaccharide, in addition, is also relevant for protection against complement-mediated killing.[4] It is of note that the transport of proteins and effectors to the environment is key to facilitate infection, competition and/or adaptation. In order to do so, bacteria employ secretion systems, complex nanomachineries that, in the case of Gram-negative bacteria, span both inner and outer membranes. Up to eleven different secretion systems have now been identified, whose functions range from injecting toxins directly into target cells to secreting macromolecules into the immediate environment of the cell.[5] *A. baumannii* has been reported to harbor type I, II, IV, V, and VI secretion systems, attesting to its requirement for versatility when it comes to interactions with its surroundings.[2,6–9] The type II secretion system (T2SS), in particular, plays a key role in *A. baumannii*'s infectivity and colonization strategies; it is a multi-protein complex that secretes fully folded proteins through both bacterial membranes using a piston-like system. The T2SS in *A. baumannii* has 11 components identified to date, including the secretin (GspD), a β-barreled assembly that forms a pore on the outer membrane through which toxins and effectors are transported, and a pseudopilus (GspG, GspH, GspI, GspJ, and GspK) that polymerizes to push the effector through the pore, using the energy of a cytoplasmic ATPase (GspE). In the inner-membrane, GspC, GspF, GspL, and GspM form a platform that connects the periplasm with the cytoplasm[10–12] (Figure S1).

Five different effectors have been reported to be secreted through the T2SS of *A. baumannii*, three of which are lipases (LipA, LipH, and LipAN), one protease (CpaA), and one adhesin (InvL). CpaA is the most extensively characterized virulence factor of the system, with roles linked to deregulation of human

All rights are reserved, including those for text and data mining, AI training, and similar technologies.

Please cite this article in press as: de Oliveira Silva et al., Architecture of an embracing lipase-foldase complex of the type II secretion system of *Acinetobacter baumannii*, Structure (2025), https://doi.org/10.1016/j.str.2024.12.022

blood coagulation and cleavage of glycoproteins involved in activation of the complement system.[13–15] InvL is an adhesin implicated in uropathogenesis in a murine catheter-associated urinary tract infection (UTI) model that can bind extracellular matrix components and adhere to urinary cell lines *in vitro*.[16] LipH and LipAN have been shown to have lipase and phospholipase activities, respectively, but further studies are needed to confirm their roles in *A. baumannii* virulence.[6,17] LipA, on the other hand, is required for lipid utilization and *in vivo* fitness in a neutropenic murine bacteremia model[4,6]; in addition, it supports colonization,[4] likely due to adaptation to different lipidic landscapes.[18] Furthermore, a growing body of evidence suggests that extracellular lipases are essential for biofilm formation and composition.[19–25]

Lipases are frequently classified into families and subfamilies based on sequence similarities and biochemical properties. Many lipases from clinically relevant bacteria belong to subfamilies I.1 and I.2, and share conserved characteristics such as calcium-binding sites, disulfide bonds, and the requirement of an accessory protein to achieve their final folds in the periplasm prior to secretion.[26,27] These accessory proteins are known as lipase-specific foldases, or Lifs, that form a unique class of inner membrane-anchored steric chaperones that do not present any significant level of homology to other protein families, and assist their cognate lipases to overcome the final energetic barrier in their folding pathway. Their action allows their cognate lipases to achieve their active form and to subsequently be secreted through the T2SS.[4,28–37] Despite efforts to elucidate the role and nature of the interactions between these proteins, the mechanisms by which the foldase assists the lipase to transit from a near-native conformation to its final, active form are still unknown. It has been proposed that the foldase could facilitate the opening of the lid that covers the lipase's active site, based on molecular dynamics simulations.[38] These computational analyses are, however, biased by the limited structural information available.

The important role played by LipA in *A. baumannii* virulence makes it an interesting potential target for novel antibacterial development, vaccinology, and/or antibody treatment strategies. However, the small number of studies concerning structure and function of lipase-foldase complexes have hampered these pursuits. Here, we report the crystal structure of *A. baumannii* LipA in complex with LipB. The interaction mode is starkly different from what has been observed in most effector-chaperone complexes involved in other secretion systems, in that instead of interacting just with a specific region of the effector, LipB surrounds LipA almost entirely, sharing with it a vast interaction region. This arrangement has been characterized in only one other system, the complex between the I.2 subfamily lipase and its cognate foldase of *Burkholderia glumae*.[39] Notably, in the T2SS of *A. baumannii*, LipA is active only while bound to LipB, displaying substrate promiscuity toward fatty acids of different lengths. An extensive bioinformatic analysis of LipB-like foldases reveals that this family of proteins is widespread over different proteobacterial classes and they could share similar architectures. By using a combination of structural and sequence analyses, we identify conserved residues that can be key for binding and activation of LipA by LipB, revealing surfaces that could be used as targets for disruption of T2SS chaperone-lipase complexes in different bacterial taxa.

RESULTS

Distribution of foldase sequences

Lipase-specific foldases form a unique class of steric chaperones that are not yet fully understood, and LipA is one of the few T2SS effectors known to use a periplasmic chaperone in its folding pathway.[6] In order to understand the distribution of this family of chaperones, we initially generated sequence similarity networks (SSN) using an enzyme function initiative-enzyme similarity tool (EFI-EST).[40] Seven hundred and thirty-six LipB homologs were obtained from the UniRef90 database, and thirteen clusters of sequences grouped by similarity were selected for further analyses (Figure 1). To evaluate if the selected sequences belonged to foldases associated to lipases potentially secreted by a T2SS, we also evaluated the co-occurrence of *lipA* and *gspD* within the selected genomes. This confirmed the presence of genes encoding GspD in genomes from representatives of each cluster, indicating the co-occurrence of T2SS and lipase-specific foldases. Notably, lipase-encoding genes are located upstream from foldase genes in species from all clusters except for 7 and 9. In cluster 7, which includes *A. baumannii*, *lipA* is located downstream of *lipB*, the gene encoding its foldase. In cluster 9, no lipase-encoding genes could be identified either directly upstream or downstream of the foldase genes, potentially indicating a different role for this homolog of LipB (Figure S2). For this reason, this cluster was excluded from further analyses.

Most foldase sequences were identified in Proteobacteria, most notably in γ-proteobacteria, β-proteobacteria, and δ-proteobacteria (Figure 1). Within γ-proteobacteria, we found clusters of sequences from the orders Pseudomonadales (clusters 1, 2, 3, 8, and 10), Moraxellalles (clusters 6 and 7), and Vibrionales (clusters 12 and 13), including species from notable genera such as *Acinetobacter*, *Pseudomonas*, *Psychrobacter*, *Marinobacter*, and *Vibrio*. Two clusters from β-proteobacteria consisted of foldases from Burkholderiales and Neisseriales (clusters 4 and 11), such as *Burkholderia* and *Chromobacterium*. The single cluster of δ-proteobacteria was composed of Myxococcales (cluster 5), that includes *Corallococcus* and *Sorangium*. Members of all aforementioned orders have been characterized as biofilm-producing bacteria with either twitching or swarming motilities,[41–53] and studies in various bacterial species have demonstrated that secreted lipases can be determinant factors in biofilm formation and composition,[19,22–25,28,54,55] making them interesting targets for biofilm-inhibiting strategies.

It is widely accepted that the RXXFDY(F/C)L(S/T)A motif is conserved among lipase-specific foldases,[32] and mutations in the highly conserved tyrosine or serine residues in this motif in Lif of *P. aeruginosa* were shown to practically abolish the foldase's capacity to maintain LipA's activity and to reduce the affinity between the foldase and the pre-active lipase.[56,57] Our sequence analysis suggests there is a much larger variation between different clusters. Through multiple sequence alignments within the nodes in each cluster, we identified specific variations of this motif (Table S1). Previous studies have demonstrated that Lif from *P. aeruginosa* can substitute for the one from *P. alcaligenes*, but not the ones from *B. glumae* or *A. calcoaceticus*.[58] In our analysis, Lifs from *P. aeruginosa* and *P. alcaligenes* localize to the same cluster, while the

Please cite this article in press as: de Oliveira Silva et al., Architecture of an embracing lipase-foldase complex of the type II secretion system of *Acinetobacter baumannii*, Structure (2025), https://doi.org/10.1016/j.str.2024.12.022

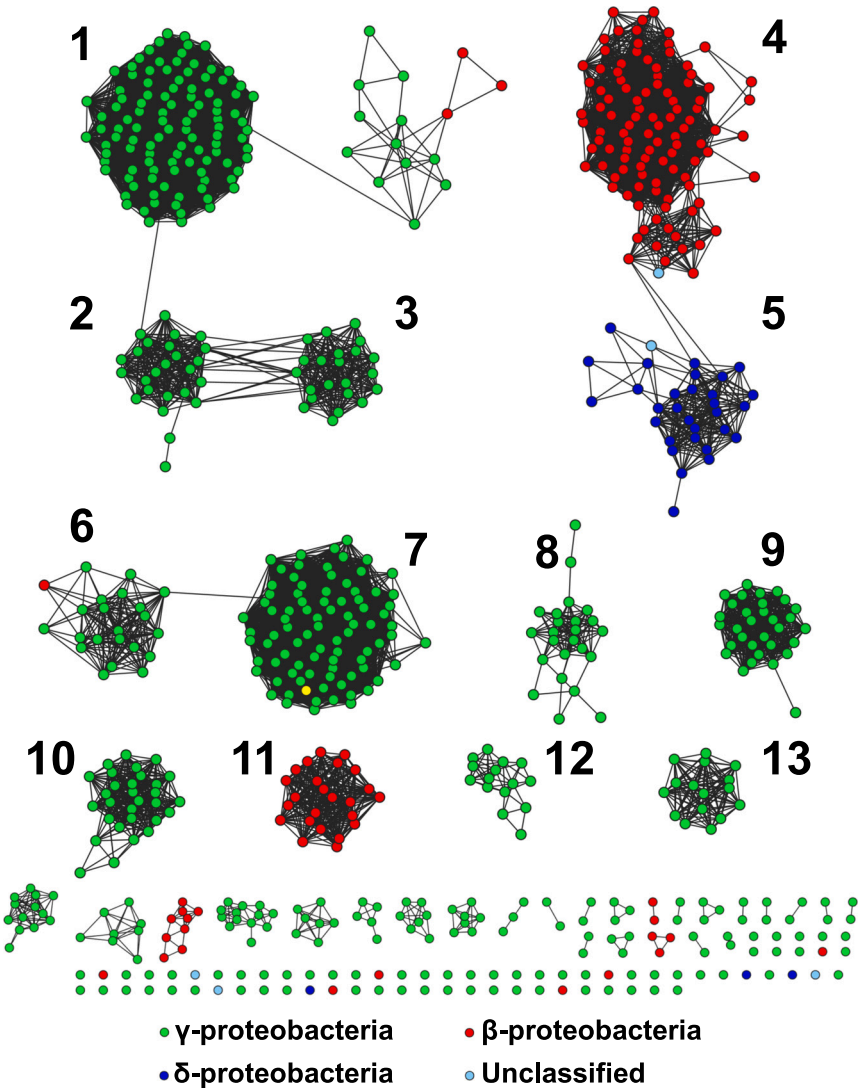

Figure 1. Distribution of Lifs and the Lif conserved motif

Sequence similarity networks for lipase-specific foldases were generated by comparing LipB from *A. baumannii* DSM30011 with the UniRef90 database. Clusters with more than 15 nodes were selected for analysis. Nodes were colored according to the taxonomic class of species to which the sequences belong (legend underneath); the node containing the *A. baumannii* sequence is colored in yellow.

homologs in *Burkholderia* and *Acinetobacter* are in separate clusters. Thus, it is likely that as bacteria adapted to new niches, lipases developed different biochemical properties, including substrate specificities, leading Lifs to adjust in order to accommodate these changes.

LipA is stable and active only in the presence of LipB

In order to further address the question of Lif-lipase recognition, we set out to structurally and enzymatically characterize the LipA-LipB complex from *A. baumannii*. We initially expressed LipA either in the presence or the absence of $LipB_{29}$, a soluble form of LipB lacking the first 28 residues, which comprise the transmembrane anchor region (Figure 2A). Overexpression of LipA in *Escherichia coli* without LipB resulted in insoluble samples, in line with what was observed before for foldase-dependent lipases from various *Pseudomonas* species,[33,56,59] that formed inclusion bodies with very low lipase activity or none at all. This issue was overcome by co-expressing LipA and $LipB_{29}$, which led to the purification of an apparent 1:1 complex after nickel affinity chromatography and gel filtration. This stoichiometry was confirmed by SEC-RALS/LALS (size exclusion chromatography coupled to right angle light scattering and low angle light scattering) of the pure sample, which showed that the complex can adopt two forms, with calculated molecular masses corresponding to a heterodimer (68.10 ± 1.15 kDa; hydrodynamic radius: 3.58 ± 0.09 nm) and a heterotetramer (135.36 ± 1.13 kDa; hydrodynamic radius: 6.48 ± 1.20 nm), indicating that not only the 1:1 complex but also a 2:2 complex can form spontaneously (Figure 2B). Moreover, the thermostability of the heterodimer assayed by differential scanning fluorimetry indicated an apparent melting temperature of 65.5°C (Figure S3).

In order to verify if LipA was active in the foldase-bound form, we employed a colorimetric activity assay using *para*-nitrophenyl-butyrate (pNPB) as a substrate. An initial analysis confirmed that both the heterodimer and the heterotetramer were similarly active, so only data relative to the dimer will be reported here. To further characterize the enzymatic activity of the $LipB_{29}$-bound LipA complex, effects of pH and temperature were initially investigated using pNPB as a substrate (Figures 2C and 2D). Optimal activity was obtained at 40°C, with 40% activity retained up to 60°C. The highest activity was observed in acidic pH values, with optimal activity achieved at pH 6.5. Furthermore, we investigated LipA's substrate preference using *para*-nitrophenol-derived substrates of different chain lengths. The highest measured activity was obtained using the short-chain substrate pNPB (C4:0), but LipA's ability to catalyze the hydrolysis of medium- and long-chain substrates was also evident (Figure 2E). Kinetic assays of pNPB cleavage under optimal conditions revealed apparent K_m and K_{cat} values of 237.67 ± 24.47 μM and 28.79 ± 1.65 s^{-1}, respectively (Figure 2F). The low K_m and high K_{cat} values indicate that LipA is a highly efficient enzyme. Its ability to hydrolyze substrates of varied chain lengths, as well as to work under higher temperatures and lower pHs could point to it being a very useful asset for the pathogen during challenges imposed by the host, such as nutrient limitation as well as acidic or heat stress.[60–62]

Please cite this article in press as: de Oliveira Silva et al., Architecture of an embracing lipase-foldase complex of the type II secretion system of *Acinetobacter baumannii*, Structure (2025), https://doi.org/10.1016/j.str.2024.12.022

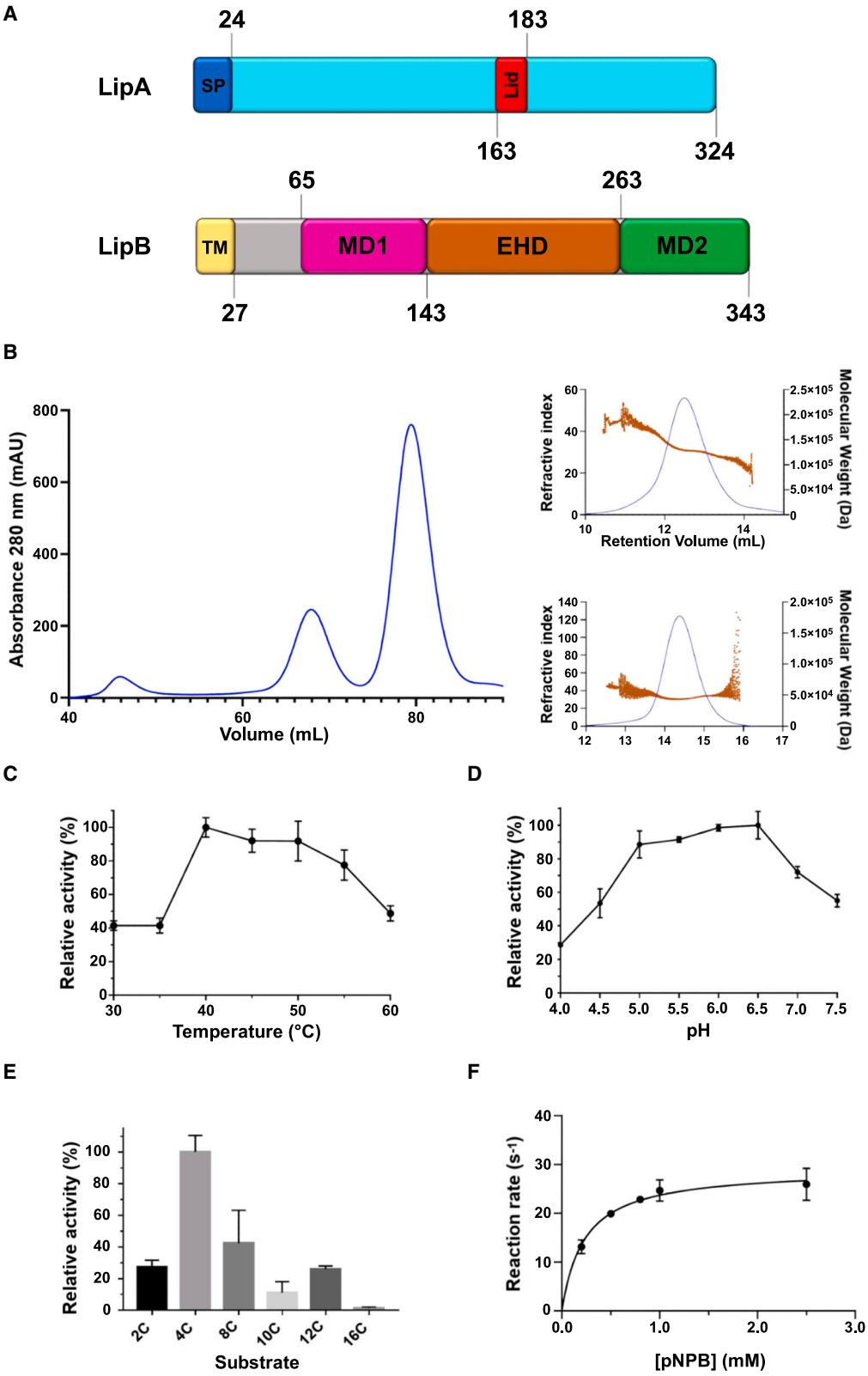

Figure 2. Characterization of LipA bound to LipB

(A) Schematics of subdomain organization of the lipase and the foldase. MD1, mini-domain 1; EHD, extended helical domain; MD2, mini-domain 2; TM, transmembrane helix; SP, signal peptide.

(legend continued on next page)

Please cite this article in press as: de Oliveira Silva et al., Architecture of an embracing lipase-foldase complex of the type II secretion system of *Acinetobacter baumannii*, Structure (2025), https://doi.org/10.1016/j.str.2024.12.022

CellPress

Structure determination of the LipA-LipB complex

Initial attempts to crystallize the LipA-LipB$_{29}$ complex were unsuccessful. We subsequently submitted LipA-LipB$_{29}$ to limited proteolysis with multiple proteases followed by mass spectrometry in order to identify a crystallizable form of the complex. These analyses indicated that region 29–51, for which no secondary structure prediction could be obtained, was rapidly proteolyzed. The LipB form lacking this unstructured region was the most abundant form after proteolysis, indicating its stability and potential compactness.

We thus generated a new, shorter LipB-expressing clone and purified the complex as described for the longer form in the methods section. The purified complex was submitted to crystallization screenings at the automated protein crystallization facility (ROBOLAB) at the LNBio, CNPEM. Initial crystallization conditions were improved by manual refinement, yielding hexagonal-shaped crystals. X-ray data were collected at the Sirius synchrotron in Campinas, Brazil. These crystals initially diffracted to very low resolution, prompting further optimization using microseed matrix seeding. This process yielded a single crystal that diffracted to 3.17 Å. The crystal belonged to space group $P3_221$ and contained one LipA-LipB heterodimer in the asymmetric unit. Molecular replacement trials using a lipase-foldase structure from *B. glumae* (PDB: 2ES4)[39] (overall sequence identity to *A. baumannii* LipA-LipB ~29%) or that of an unchaperoned lipase from *P. aeruginosa* (PDB: 1EX9)[63] (sequence identity to *A. baumannii* LipA ~49%) did not yield promising initial results. We thus generated an AlphaFold model of *A. baumannii* LipA-LipB and used it for molecular replacement. This approach led to an initial R_{free} of 38% that was further improved to 29% after several rounds of refinement. Data collection and refinement statistics can be found in Table 1.

LipB surrounds LipA in a stabilizing embrace

Each copy of the complex displays LipA bound to LipB$_{52}$ in a 1:1 ratio, confirming the SEC-RALS results. The structure is highly unusual for a chaperone-effector complex, in that LipB$_{52}$ consists of an extended α-helical architecture that embraces LipA on the outside of the lipase (Figure 3A). Surface analyses using PDBePISA indicate a large interface area of 3,318 Å^2, with roughly 28% of the residues of each protein forming the protein-protein interface. This is in clear contrast to structures of other chaperone-effector complexes in secretion systems, where the chaperone interacts with a limited section of the effector (see the following text).[64–70] The only exception is the previously reported lipase-foldase complex from *B. glumae,*[39] where the lipase is also surrounded by an extended helical partner; however, the positions, extensions and kinks of the helices of the chaperones display differences (Figures S4A and S4B), providing a potential explanation for the initial unpromising results obtained for our molecular replacement efforts when we employed the *B. glumae* structure (aforementioned). This embracing architecture could explain how the lipase retains its activity even at higher temperatures and under extreme acidic conditions, when in complex with its partner foldase. It is of note that lipases from *B. glumae* and *P. aeruginosa* interact with their cognate foldases with affinities in the nanomolar range,[39,56] lending support to the importance of the stabilizing role of the chaperone.

LipA displays a typical α/β hydrolase fold with six β-strands forming a central parallel β-sheet, surrounded by eight α-helices (Figure 3B). According to the modular classification for hydrolases, this lipase can be classified as a Core + Lid (β+1 → β+2) hydrolase,[71] presenting a lid region formed by a hydrophobic helix (α5). The function of the lid in lipases is to control substrate access to the active site, and it can often be a determinant of substrate specificity, thermostability and activity.[72] In the LipA-LipB structure, the lid does not make contact with LipB and is neither in fully "open" or "closed" conformations, as seen in other lipase structures, adopting instead an intermediate conformation that partially exposes the active site (Figure S4C). In fact, previous molecular dynamics simulations have shown that an open conformation is the most favorable when the lipase is bound to the foldase in *P. aeruginosa*.[38] The active cleft is at the bottom of a funnel decorated by hydrophobic side chains that could potentially accommodate the lipidic substrate (Figure 3C). The catalytic serine of LipA is located in a nucleophilic elbow between β3 and α3 and is part of a classical catalytic triad (Ser121-His290-Asp268), expected to be involved in the nucleophilic attack that leads to substrate hydrolysis. His122 and Met51 are proximal to the catalytic site and are in equivalent positions to residues that form the oxyanion hole in the structure of the homologous lipase in *P. aeruginosa*, in which they are required to stabilize intermediates during catalysis.[63] Previous studies have suggested that activation of LipA by LipB could be linked to the formation of a short β-hairpin in the N-terminal region of the lipase,[56] but that does not seem to be the case in our structure. Instead, the equivalent region remains unstructured in the active lipase (Figure S4D).

The LipA-LipB interface reveals details of foldase dependence by LipA

LipB$_{52}$ is composed of 11 helices, organized into an N-terminal globular mini-domain (MD1, helices α1–α3), a C-terminal globular mini-domain (MD2, helices α9–α11) and a connecting extended helical region (EHD) (Figures 2A and 4A). The large interface between LipB and LipA involves more than 70 residues from each protein. Assuming that residues that are highly conserved would play an important role in stabilizing the interaction, we aligned representative LipB sequences from each

(B) The LipA-LipB complex elutes in two peaks in size-exclusion chromatography (left), which were characterized as a (I) heterotetramer (molecular weight: 135.36 ± 1.13 kDa; hydrodynamic radius: 6.48 ± 1.20 nm) and a (II) heterodimer (molecular weight: 68.10 ± 1.15 kDa; hydrodynamic radius: 3.58 ± 0.09 nm) by SEC-RALS/LALS (right). Data are represented as mean (n = 3).

(C and D) Effects of temperature (C) and pH (D) on lipase activity were assayed using pNPB as substrate. Data are represented as mean ± SD (n = 3).

(E) Substrate preference was evaluated using *para*-nitrophenyl esters of different chain lengths. Relative activity (%) was calculated using the highest activity average value in each experiment, which was set as 100%. Data are represented as mean ± SD (n = 3).

(F) Kinetic parameters were determined for pNPB cleavage under optimal conditions. (Apparent K_m) = 237.67 ± 24.47 μM; K_{cat} = 28.79 ± 1.65 s^{-1}. Data are represented as mean ± SD (n = 3).

Please cite this article in press as: de Oliveira Silva et al., Architecture of an embracing lipase-foldase complex of the type II secretion system of *Acinetobacter baumannii*, Structure (2025), https://doi.org/10.1016/j.str.2024.12.022

Table 1. Data collection, phasing, and structure refinement statistics

Data collection	
X-ray source (Beamline)	Sirius (Manacá)
Detector	Pilatus 2M
Wavelength (Å)	0.97718
Scan-range (°)	360
Oscillation (°)	0.1
Space group	$P3_221$
a (Å)	133.69
b (Å)	133.69
c (Å)	139.71
α (°)	90
β (°)	90
γ (°)	120
Mosaicity (°)	0.358
Overall resolution (Å)	48.30–3.17
No. observed/unique reflections	454,688/23,444
High resolution shell (Å)	3.37–3.17
Completeness (%) (last shell)	96.2(97.4)
R_{sym} (%) (last shell)	61.3 (1003.2)
$I/\sigma(I)$ (last shell)	5.57 (0.30)
$CC_{1/2}$	99.7 (21.4)
Wilson plot B-factor (Å^2)	104.87
Molecular replacement	
Phaser RFZ/TFZ/LLG	4.20/25.50/435.44
Refinement	
Initial R_{work}/R_{free} (%)	33.31/38.42
Final R_{work}/R_{free} (%)	27.71/29.50
B-factor (Å^2) global	151.15
B-factor (Å^2) protein	151.34
B-factor (Å^2) waters	92.58
B-factor (Å^2) ligands Ca	109.33
B-factor (Å^2) ligands Cl	123.26
Stereochemical quality	
RMS deviation, bond lengths (Å)	0.006
RMS deviation, bond angles (°)	1.265
No. of atoms	4621
No. of protein atoms	4605
No. of calcium atoms	1
No. of chlorine atoms	1
No. of water molecules	15
Residues in most favored/allowed region of Ramachandran plot (%)	99.80
Clashscore	1.4
Sidechain outliers	0.4%

cluster in our SSN to that of *A. baumannii* and calculated sequence conservation using ConSurf.[73] Out of 79 interfacing residues from LipB, only 24 were conserved across representatives of all clusters, 13 of these participating in interactions (Table S2). Although interacting residues are distributed in the subdomains, roughly half of the total conserved residues and polar interactions detected are localized in MD1, highlighting the importance of this mini-domain. It is of note that the conserved Lif motif in MD1 is essential for LipB function since mutagenesis of single residues practically abolishes the activity of the LipA-LipB complex of the T2SS of *P. aeruginosa*.[57]

The same analysis was performed with the cognate lipases, revealing 24 conserved interfacing residues in LipA. By combining the sequence conservation analyses of LipA and LipB, we were able to identify conserved interactions across different bacterial classes (Figure S5). Two conserved interactions occur between MD1 of LipB and α8 of LipA (Ser66/LipB:Arg318/LipA and Asn73/LipB:Arg313/LipA) (Figure 4B), as well as MD2 of LipB and helices α2 and α3 of LipA (Arg325/LipB:Glu97/LipA and Thr328/LipB:Tyr129/LipA) (Figures 4C and 4D). Notably, LipA's Tyr129 is located in the same helix as the catalytic serine, which could suggest a role for this interaction in the lipase-activating function of the foldase. The relevance of one of the interactions mentioned previously was demonstrated in a previous study in a homolog Lipase-Lif complex from *Acinetobacter* sp. XMZ-26, in which a substitution of Arg325 in the foldase into any other amino acid was enough to hinder foldase-lipase interactions in co-precipitation and in yeast two-hybrid assays,[29] possibly due to the disruption of the interactions with Glu97 in α2 of LipA. The conservation of interactions in this and the other aforementioned positions indicate not only that the MD1 and MD2 regions of LipB play key roles in the interaction with LipA from *A. baumannii*, but also that homologous residues should be essential for lipase-folding interactions in numerous bacteria identified in the aforementioned clusters.

DISCUSSION

Secretion systems mediate transport of effectors through bacterial membranes, thus frequently playing key roles in infection and/or colonization processes. Effectors often require the participation of foldases or chaperones for stabilization and activity maintenance; however, these auxiliary proteins employ different strategies to recognize their cognate partners. In the well-studied T3SS, for example, effectors are stabilized by chaperones within the bacterial cytoplasm and are transported in unfolded form through the polymerized needle structure.[74,75] Interestingly, T3SS chaperone-effector complexes often involve small interaction regions, as is the case for ExoU:SpcU of *P. aeruginosa*, as well as SipA:InvB of *S. enterica*. ExoU is a highly active phospholipase, whose N-terminal region is stabilized by hydrophobic patches in SpcU[64]; SipA is an actin-binding protein that is contacted by InvB through an extended C-terminal loop region[65] (Figure 5, top). Such limited interactions could facilitate the highly regulated release and unfolding steps that must occur prior to threading of the effector through the interior of the needle.[75]

In order to be secreted in folded form through the *A. baumannii* T2SS, effectors are translocated through the inner bacterial membrane using the Tat or Sec systems[77] and require a chaperone or foldase recognition step in the periplasm. These are often membrane-associated proteins that are not themselves secreted through the system and maintain effector stability and activity. This differential mode of action is reflected in the nature

Please cite this article in press as: de Oliveira Silva et al., Architecture of an embracing lipase-foldase complex of the type II secretion system of *Acinetobacter baumannii*, Structure (2025), https://doi.org/10.1016/j.str.2024.12.022

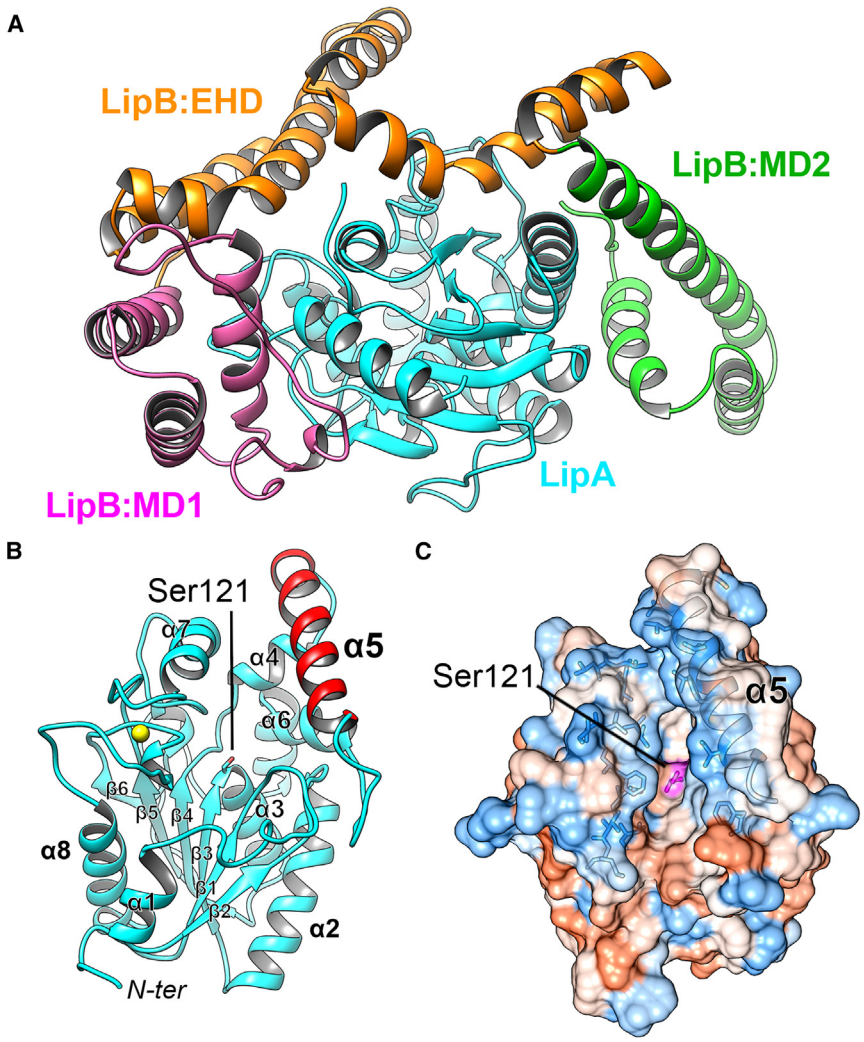

Figure 3. LipB embraces LipA

(A) Structure of LipA-LipB complex from *A. baumannii* described in this work. LipB plays a foldase role by positioning itself around LipA as if in an embrace, forming a wide contact surface that is atypical for chaperone-effector complexes in secretion systems.

(B) LipA presents a classical α/β hydrolase fold in which a central β-sheet is surrounded by α-helices, one of them being the lid (α5, red), capable of covering the active site, where the catalytic Ser121 is located in a nucleophilic elbow between a helix and a strand. The yellow sphere represents a calcium atom.

(C) Surface diagram of LipA where acidic residues are indicated in red and basic residues in blue. The active site, located at the bottom of a funnel, is indicated in purple.

of the complexes themselves. CpaA, a protease secreted by *A. nosocomialis*, surrounds the chaperone CpaB, which stabilizes mostly its central region,[66] while the LipA-LipB complex from *B. glumae* is highly reminiscent of the one from *A. baumannii* solved in this work, where the lipase effector is surrounded by the partner. Nevertheless, the "embrace" provided by LipB guarantees LipA stability and activity; this is supported by our *in vitro* data reported here, that confirms that the expression of LipA in the absence of LipB leads to an aggregated, inactive lipase. The stability of such an embrace raises questions regarding the mechanism of LipA secretion through the T2SS system. Unlike in the case of protease- chaperone complexes, where the protease can remove its cognate chaperone autoproteolytically, the separation of the LipA-LipB complex most probably requires its interaction with base components of the T2SS secretion machinery and other periplasmic factors. In *P. aeruginosa*, GspC, GspL (XcpY), and GspM (XcpZ), all of which are anchored in the inner membrane (Figure S1), have been shown to participate in different stages of effector recruitment prior to secretion, with the latter two undergoing oligomerization and heterodimerization steps that are triggered upon effector recognition.[78,79] It is tempting to propose that, in the case of *A. baumannii*, LipA can potentially directly contact the components mentioned previously and subsequently be appropriately positioned at the tip of the pseudopilus. However, this still leaves open the question of how LipA and LipB are separated, and if LipB is recycled for further use (or proteolyzed) after LipA is secreted. Further work is required to pinpoint the stepwise mechanism of this process.

The Lif-lipase systems from *B. glumae* and *P. aeruginosa* have been used as models to understand the role of foldases in lipase activation. The lipase from *B. glumae* belongs to subfamily I.2, and these enzymes are known to have shorter lid helices and an insertion between strand β5 and helix α7, thus presenting two antiparallel β-strands in comparison to lipases from subfamily I.1.[63,80] LipA from *P. aeruginosa* is the prototypical lipase from subfamily I.1, but no structure of this lipase in complex with its foldase is available. These differences may explain why, despite the similarities in sequence and overall fold, the structures of the LipA-LipB complex from *B. glumae* and LipA from *P. aeruginosa* were less useful as models for molecular replacement trials for the *A. baumannii* structure reported here. In fact, cognate lipases of foldases from most clusters in our bioinformatic analysis classify as being members of subfamily I.1. Thus, the LipA-LipB complex of *A. baumannii* presented here includes a lipase from subfamily I.1 and could facilitate further structural studies of similar complexes.

Lifs from closely related species have been shown to activate each other's lipases, while Lifs from more phylogenetic distant species are not able to.[58] Our sequence analysis agrees with these studies, separating Lifs that cannot substitute for each other into different clusters. The conserved Lif motif, critical for foldase function, presents cluster-specific variations, and these changes may be linked to the specificity for the cognate lipases, in order to maintain the high affinity that has been observed in *P. aeruginosa* and *B. glumae* (clusters 1 and 11,

Please cite this article in press as: de Oliveira Silva et al., Architecture of an embracing lipase-foldase complex of the type II secretion system of *Acinetobacter baumannii*, Structure (2025), https://doi.org/10.1016/j.str.2024.12.022

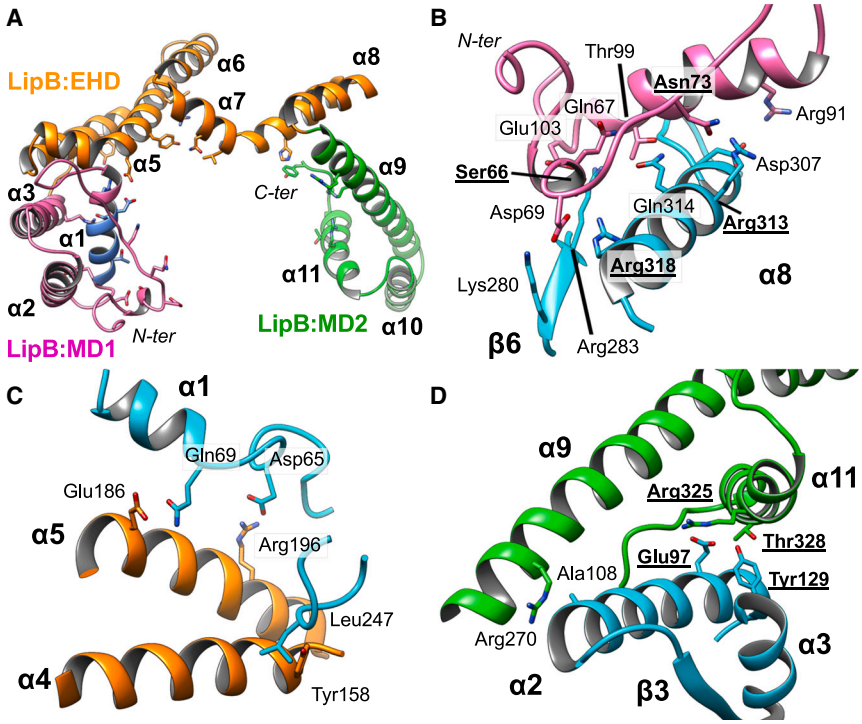

Figure 4. The LipA-LipB interaction surface

(A) Structure of LipB showing residues that interact with LipA. Note that all three domains of the foldase contribute residues toward the interaction with LipA, providing stability to a vast region of the lipase. The conserved Lif motif is highlighted in blue.

(B–D) Conserved interactions between LipA (cyan) and LipB subdomains MD1 (magenta), EHD (orange), and MD2 (green). Residues involved in conserved interactions are in bold/underlined.

respectively). Only one residue was found to be invariable across all clusters, Tyr96. Mutations of this residue greatly decreased the affinity between the foldase and the lipase and were enough to disrupt lipase activation.[57] Interestingly, neither in *A. baumannii* nor in *B. glumae*'s lipase-foldase structures does this residue seem to be directly interacting with the lipase, reinforcing the idea that it exerts a long-range effect on LipA.[56] In addition, through sequence conservation and structure analyses, we identified four conserved interactions between LipA and LipB that could be crucial for foldase activity, one of which was experimentally demonstrated in a study in a homologous system (Arg325/LipB:Glu97/LipA, Figure 4D). We hypothesize that the conserved interactions identified here are essential for complex formation and for the Lif embrace observed in the LipA-LipB structure.

A. baumannii's ability to persist in tissues is key for the establishment of chronic infections. Two main characteristics are linked to this capability: its capacity to resist antibiotics with different mechanisms of action, and to adapt to modifications in its microenvironment.[2] *A. baumannii* is a colonizer of the human respiratory tract, and thus is commonly found in airway surface liquid (ASL). Studies performed with pneumonia patients in intensive care unit (ICU) settings indicated that the pH of respiratory mucus can vary throughout the infection process, maintaining stability during the initial colonization phases but becoming acidic once pneumonia is established[81]; ASL of cystic fibrosis patients, for example, is both dehydrated and acidic.[82] In order to adapt to such modifications, *A. baumannii* has been reported to display reversible phases, even introducing in-host mutations in key proteins.[83] In addition, LipA, a virulence factor that plays a role in colonization and infection,[4] maintains close to 100% lipid-hydrolysis activity at pH 5.0 and still displays up to 30% activity at pH 4.0, even in its LipB-bound, unsecreted form. These abilities attest to LipB's capacity to maintain LipA in active form by stabilizing the lateral region of the lipase, allowing unencumbered active site access (Figure 3B), thus supporting *A. baumannii*'s great versatility as a pathogen in microenvironments that are constantly changing.

RESOURCE AVAILABILITY

Lead contact

Further information and requests for resources and reagents should be directed to and will be fulfilled by the lead contact, Andréa Dessen (andrea.dessen@cnrs.fr).

Materials availability

This study did not generate new unique reagents.

Data and code availability

The atomic coordinates and structure factors for the structure of the *A. baumannii* LipA-LipB complex have been deposited in the Protein DataBank and are publicly available as of the date of publication, with the accession number 9G8U. This paper does not report original code. Any additional information required to reanalyze the data reported in this paper is available from the lead contact upon request.

ACKNOWLEDGMENTS

We acknowledge support to AD from the Laboratoire International Associé BACWALL (CNRS), and grants from the São Paulo Research Foundation (FAPESP) 2011/52067-6 and 2017/12436-9. YROS was supported by a PhD fellowship 2018/04344-0 within grant 2017/12436-9 from FAPESP. This work used the platforms of the Grenoble Instruct-ERIC centre (ISBG; UAR 3518 CNRS-CEA-UGA-EMBL) within the Grenoble Partnership for Structural Biology (PSB), supported by FRISBI (ANR-10-INBS-05-02) and GRAL, financed within the University Grenoble Alpes graduate school (Ecoles Universitaires de Recherche) CBH-EUR-GS (ANR-17-EURE-0003). The IBS

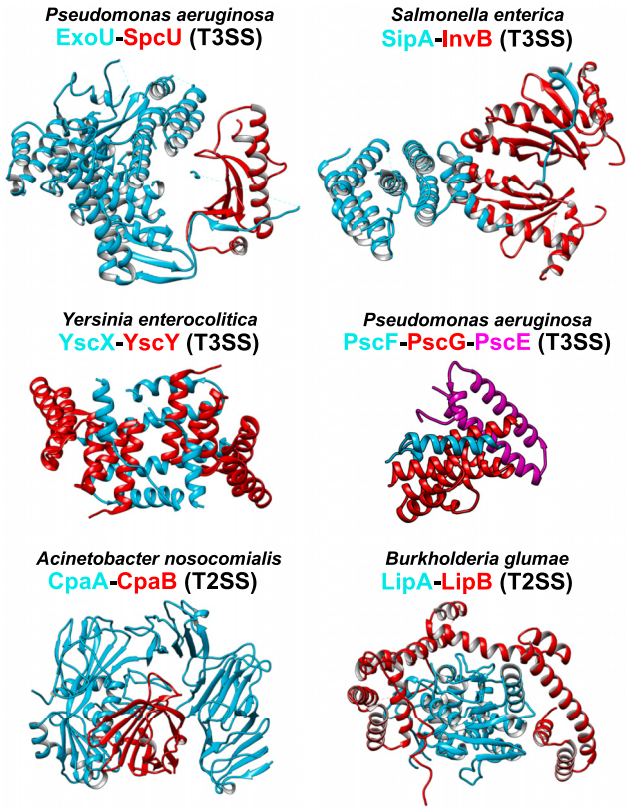

Figure 5. Structures of chaperone-bound effectors in T2SS and T3SS

In the structures of T3SS chaperone-effector complexes, small regions of the chaperones contact the effectors, as seen for ExoU-SpcU[64] (PDB: 4AKX, T3SS class Ia chaperone), SipA-InvB[65] (PDB: 2FM8, T3SS class Ib chaperone), YscX-YscY[76] (PDB: 7QIH, T3SS class II chaperone), and PscF-PscG-PscE[67] (PDB: 2UWJ, T3SS class III chaperones). In T2SS, the effector CpaA embraces the chaperone CpaB[66] (PDB: 6O38), while the chaperone LipB has been shown to embrace the effector LipA in *B. glumae*[39] (PDB: 2ES4). Effectors are colored cyan, chaperones are colored red.

acknowledges integration into the Interdisciplinary Research Institute of Grenoble (IRIG, CEA). This work also made use of the MANACÁ beamline of the Brazilian Synchrotron Light Laboratory (LNLS-Sirius), the Spectroscopy and Calorimetry Facility (LEC), the ROBOLAB automatic crystallization facility of the LNBio, and facilities of the Brazilian Biorenewables National Laboratory (LNBR). BFM staff, as well as Luca Signor (IBS), are acknowledged for their assistance with experiments. The LNLS, LNBR and LNBio are operated by the Center for Research in Energy and Materials (CNPEM) for the Ministry for Science, Technology and Innovation (MCTI, Brazil).

AUTHOR CONTRIBUTIONS

A.D. conceived the project. Y.R.O.S., D.M.T., L.M.Z., and A.D. designed the experiments. Y.R.O.S. performed protein purification, crystallization, data collection, and biophysical studies. C.C.-M. processed data, solved and refined the crystal structure. D.M.T. performed molecular cloning and data collection. R.R.M. and L.M.Z. performed substrate binding and kinetic studies. Y.R.O.S. and A.D. wrote the manuscript.

DECLARATION OF INTERESTS

The authors declare no competing interests.

STAR★METHODS

Detailed methods are provided in the online version of this paper and include the following:

- KEY RESOURCES TABLE
- EXPERIMENTAL MODEL AND STUDY PARTICIPANT DETAILS
- METHOD DETAILS
  - Construct design
  - Protein expression, purification and crystallization
  - Limited proteolysis
  - Light Scattering
  - Biochemical characterization
  - Sequence analyses
  - Data collection, structure determination and refinement
- QUANTIFICATION AND STATISTICAL ANALYSIS

SUPPLEMENTAL INFORMATION

Supplemental information can be found online at https://doi.org/10.1016/j.str.2024.12.022.

Received: August 7, 2024
Revised: October 23, 2024
Accepted: December 28, 2024
Published: February 3, 2025

REFERENCES

1. Giammanco, A., Calà, C., Fasciana, T., and Dowzicky, M.J. (2017). Global assessment of the activity of tigecycline against Multidrug-Resistant Gram-negative pathogens between 2004 and 2014 as part of the tigecycline evaluation and surveillance trial. mSphere *2*, e00310. https://doi.org/10.1128/msphere.00310-16.
2. Harding, C.M., Pulido, M.R., Di Venanzio, G., Kinsella, R.L., Webb, A.I., Scott, N.E., Pachón, J., and Feldman, M.F. (2017). Pathogenic *Acinetobacter* species have a functional Type I Secretion System and contact-dependent inhibition systems. J. Biol. Chem. *292*, 9075–9087. https://doi.org/10.1074/jbc.M117.781575.
3. Thompson, M.G., Black, C.C., Pavlicek, R.L., Honnold, C.L., Wise, M.C., Alamneh, Y.A., Moon, J.K., Kessler, J.L., Si, Y., Williams, R., et al. (2014). Validation of a novel murine wound model of *Acinetobacter baumannii* infection. Antimicrob. Agents Chemother. *58*, 1332–1342. https://doi.org/10.1128/AAC.01944-13.
4. Johnson, T.L., Waack, U., Smith, S., Mobley, H., and Sandkvist, M. (2015). *Acinetobacter baumannii* is dependent on the Type II Secretion System and its substrate LipA for lipid utilization and *in vivo* fitness. J. Bacteriol. *198*, 711–719. https://doi.org/10.1128/JB.00622-15.
5. Filloux, A. (2022). Bacterial protein secretion systems: Game of types. Microbiology *168*, 001193. https://doi.org/10.1099/mic.0.001193.
6. Harding, C.M., Kinsella, R.L., Palmer, L.D., Skaar, E.P., and Feldman, M.F. (2016). Medically relevant *Acinetobacter* species require a Type II Secretion System and specific membrane-associated chaperones for the export of multiple substrates and full virulence. PLoS Pathog. *12*, e1005391. https://doi.org/10.1371/journal.ppat.1005391.
7. Liu, C.C., Kuo, H.Y., Tang, C.Y., Chang, K.C., and Liou, M.L. (2014). Prevalence and mapping of a plasmid encoding a Type IV Secretion System in *Acinetobacter baumannii*. Genomics *104*, 215–223. https://doi.org/10.1016/j.ygeno.2014.07.011.
8. Bentancor, L.V., Camacho-Peiro, A., Bozkurt-Guzel, C., Pier, G.B., and Maira-Litrán, T. (2012). Identification of Ata, a multifunctional trimeric autotransporter of *Acinetobacter baumannii*. J. Bacteriol. *194*, 3950–3960. https://doi.org/10.1128/JB.06769-11.
9. Le, N.-H., Pinedo, V., Lopez, J., Cava, F., and Feldman, M.F. (2021). Killing of Gram-negative and Gram-positive bacteria by a bifunctional

Please cite this article in press as: de Oliveira Silva et al., Architecture of an embracing lipase-foldase complex of the type II secretion system of *Acinetobacter baumannii*, Structure (2025), https://doi.org/10.1016/j.str.2024.12.022

cell wall-targeting T6SS effector. Proc. Natl. Acad. Sci. USA *118*, e2106555118.

10. Silva, Y.R.d.O., Contreras-Martel, C., Macheboeuf, P., and Dessen, A. (2020). Bacterial secretins: Mechanisms of assembly and membrane targeting. Protein Sci. *29*, 893–904. https://doi.org/10.1002/pro.3835.
11. Eijkelkamp, B.A., Stroeher, U.H., Hassan, K.A., Paulsen, I.T., and Brown, M.H. (2014). Comparative analysis of surface-exposed virulence factors of *Acinetobacter baumannii*. BMC Genom. *15*, 1020. https://doi.org/10.1186/1471-2164-15-1020.
12. Weber, B.S., Kinsella, R.L., Harding, C.M., and Feldman, M.F. (2017). The secrets of *Acinetobacter* Secretion. Trends Microbiol. *25*, 532–545. https://doi.org/10.1016/j.tim.2017.01.005.
13. Tilley, D., Law, R., Warren, S., Samis, J.A., and Kumar, A. (2014). CpaA a novel protease from *Acinetobacter baumannii* clinical isolates deregulates blood coagulation. FEMS Microbiol. Lett. *356*, 53–61. https://doi.org/10.1111/1574-6968.12496.
14. Haurat, M.F., Scott, N.E., Di Venanzio, G., Lopez, J., Pluvinage, B., Boraston, A.B., Ferracane, M.J., and Feldman, M.F. (2020). The glycoprotease CpaA secreted by medically relevant *Acinetobacter* species targets multiple O-linked host glycoproteins. mBio *11*, e02033-20. https://doi.org/10.1128/mBio.02033-20.
15. Waack, U., Warnock, M., Yee, A., Huttinger, Z., Smith, S., Kumar, A., Deroux, A., Ginsburg, D., Mobley, H.L.T., Lawrence, D.A., and Sandkvist, M. (2018). CpaA is a glycan-specific adamalysin-like protease secreted by *Acinetobacter baumannii* that inactivates coagulation factor XII. mBio *9*, e01606-18. https://doi.org/10.1128/mBio.01606-18.
16. Jackson-Litteken, C.D., Di Venanzio, G., Le, N.-H., Scott, N.E., Djahanschiri, B., Distel, J.S., Pardue, E.J., Ebersberger, I., and Feldman, M.F. (2022). InvL, an invasin-like adhesin, is a Type II Secretion System substrate required for *Acinetobacter baumannii* uropathogenesis. mBio *13*, e0025822. https://doi.org/10.1128/mbio.00258-22.
17. Elhosseiny, N.M., El-Tayeb, O.M., Yassin, A.S., Lory, S., and Attia, A.S. (2016). The secretome of *Acinetobacter baumannii* ATCC 17978 Type II Secretion System reveals a novel plasmid encoded phospholipase that could be implicated in lung colonization. Int. J. Med. Microbiol. *306*, 633–641. https://doi.org/10.1016/j.ijmm.2016.09.006.
18. Adams, F.G., Trappetti, C., Waters, J.K., Zang, M., Brazel, E.B., Paton, J.C., Snel, M.F., and Eijkelkamp, B.A. (2021). To Make or Take: Bacterial Lipid Homeostasis during Infection. mBio *12*, e0092821. https://doi.org/10.1128/mbio.00928-21.
19. Irudal, S., Scoffone, V.C., Trespidi, G., Barbieri, G., D'Amato, M., Viglio, S., Pizza, M., Scarselli, M., Riccardi, G., and Buroni, S. (2023). Identification by reverse vaccinology of three virulence factors in *Burkholderia cenocepacia* that may represent ideal vaccine antigens. Vaccines *11*, 1039. https://doi.org/10.3390/vaccines11061039.
20. Ma, S., Dong, Y., Wang, N., Liu, J., Lu, C., and Liu, Y. (2020). Identification of a new effector-immunity pair of *Aeromonas hydrophila* Type VI Secretion System. Vet. Res. *51*, 71. https://doi.org/10.1186/s13567-020-00794-w.
21. Tielen, P., Kuhn, H., Rosenau, F., Jaeger, K.E., Flemming, H.C., and Wingender, J. (2013). Interaction between extracellular lipase LipA and the polysaccharide alginate of *Pseudomonas aeruginosa*. BMC Microbiol. *13*, 159. https://doi.org/10.1186/1471-2180-13-159.
22. Nguyen, M.T., Luqman, A., Bitschar, K., Hertlein, T., Dick, J., Ohlsen, K., Bröker, B., Schittek, B., and Götz, F. (2018). Staphylococcal (phospho)lipases promote biofilm formation and host cell invasion. Int. J. Med. Microbiol. *308*, 653–663. https://doi.org/10.1016/j.ijmm.2017.11.013.
23. Ennouri, H., d'Abzac, P., Hakil, F., Branchu, P., Naïtali, M., Lomenech, A.M., Oueslati, R., Desbrières, J., Sivadon, P., and Grimaud, R. (2017). The extracellular matrix of the oleolytic biofilms of *Marinobacter hydrocarbonoclasticus* comprises cytoplasmic proteins and T2SS effectors that promote growth on hydrocarbons and lipids. Environ. Microbiol. *19*, 159–173. https://doi.org/10.1111/1462-2920.13547.
24. Hu, C., Xiong, N., Zhang, Y., Rayner, S., and Chen, S. (2012). Functional characterization of lipase in the pathogenesis of *Staphylococcus aureus*. Biochem. Biophys. Res. Commun. *419*, 617–620. https://doi.org/10.1016/j.bbrc.2012.02.057.
25. Rosenau, F., Isenhardt, S., Gdynia, A., Tielker, D., Schmidt, E., Tielen, P., Schobert, M., Jahn, D., Wilhelm, S., and Jaeger, K.E. (2010). Lipase LipC affects motility, biofilm formation and rhamnolipid production in *Pseudomonas aeruginosa*. FEMS Microbiol. Lett. *309*, 25–34. https://doi.org/10.1111/j.1574-6968.2010.02017.x.
26. Hitch, T.C.A., and Clavel, T. (2019). A proposed update for the classification and description of bacterial lipolytic enzymes. PeerJ *7*, e7249. https://doi.org/10.7717/peerj.7249.
27. Arpigny, J.L., and Jaeger, K.-E. (1999). Bacterial lipolytic enzymes: classification and properties. Biochem. J. *343*, 177–183.
28. Nascimento, R., Gouran, H., Chakraborty, S., Gillespie, H.W., Almeida-Souza, H.O., Tu, A., Rao, B.J., Feldstein, P.A., Bruening, G., Goulart, L.R., and Dandekar, A.M. (2016). The Type II secreted lipase/esterase LesA is a key virulence factor required for *Xylella fastidiosa* pathogenesis in grapevines. Sci. Rep. *6*, 18598. https://doi.org/10.1038/srep18598.
29. Zheng, X., Tian, J., Wu, N., and Fan, Y. (2013). Probing the molecular determinant of the lipase-specific foldase Lif26 for the interaction with its cognate Lip26. Int. J. Biol. Macromol. *53*, 54–61. https://doi.org/10.1016/j.ijbiomac.2012.11.007.
30. Martini, V.P., Glogauer, A., Müller-Santos, M., Iulek, J., de Souza, E.M., Mitchell, D.A., Pedrosa, F.O., and Krieger, N. (2014). First co-expression of a lipase and its specific foldase obtained by metagenomics. Microb. Cell Fact *13*, 171. https://doi.org/10.1186/s12934-014-0171-7.
31. Sullivan, E.R., Leahy, J.G., and Colwell, R.R. (1999). Cloning and sequence analysis of the lipase and lipase chaperone-encoding genes from *Acinetobacter calcoaceticus* RAG-1, and redefinition of a Proteobacterial lipase family and an analogous lipase chaperone family. Gene *230*, 277–286.
32. Rosenau, F., Tommassen, J., and Jaeger, K.E. (2004). Lipase-specific foldases. Chembiochem *5*, 152–161. https://doi.org/10.1002/cbic.200300761.
33. Ogino, H., Inoue, S., Yasuda, M., and Doukyu, N. (2013). Hyper-activation of foldase-dependent lipase with lipase-specific foldase. J. Biotechnol. *166*, 20–24. https://doi.org/10.1016/j.jbiotec.2013.05.002.
34. Novototskaya-Vlasova, K., Petrovskaya, L., Kryukova, E., Rivkina, E., Dolgikh, D., and Kirpichnikov, M. (2013). Expression and chaperone-assisted refolding of a new cold-active lipase from *Psychrobacter cryohalolentis* K5T. Protein Expr. Purif. *91*, 96–103. https://doi.org/10.1016/j.pep.2013.07.011.
35. Lee, J.H., Ashby, R.D., Needleman, D.S., Lee, K.T., and Solaiman, D.K.Y. (2012). Cloning, sequencing, and characterization of lipase genes from a polyhydroxyalkanoate (PHA)-synthesizing *Pseudomonas resinovorans*. Appl. Microbiol. Biotechnol. *96*, 993–1005. https://doi.org/10.1007/s00253-012-4133-x.
36. Kagami, Y., Ratliff, M., Surber, M., Martinez, A., and Nunn, D.N. (1998). Type II protein secretion by *Pseudomonas aeruginosa*: Genetic suppression of a conditional mutation in the pilin-like component XcpT by the cytoplasmic component XcpR. Mol. Microbiol. *27*, 221–233. https://doi.org/10.1046/j.1365-2958.1998.00679.x.
37. Martínez, A., Ostrovsky, P., and Nunn, D.N. (1999). LipC, a second lipase of *Pseudomonas aeruginosa,* is LipB and Xcp dependent and is transcriptionally regulated by pilus biogenesis components. Mol. Microbiol. *34*, 317–326. https://doi.org/10.1046/j.1365-2958.1999.01601.x.
38. Verma, N., Dollinger, P., Kovacic, F., Jaeger, K.E., and Gohlke, H. (2020). The Membrane-Integrated Steric Chaperone Lif Facilitates Active Site Opening of Pseudomonas aeruginosa Lipase A. J. Comput. Chem. *41*, 500–512. https://doi.org/10.1002/jcc.26085.
39. Pauwels, K., Lustig, A., Wyns, L., Tommassen, J., Savvides, S.N., and Van Gelder, P. (2006). Structure of a membrane-based steric chaperone in complex with its lipase substrate. Nat. Struct. Mol. Biol. *13*, 374–375. https://doi.org/10.1038/nsmb1065.
40. Gerlt, J.A., Bouvier, J.T., Davidson, D.B., Imker, H.J., Sadkhin, B., Slater, D.R., and Whalen, K.L. (2015). Enzyme function initiative-enzyme

Please cite this article in press as: de Oliveira Silva et al., Architecture of an embracing lipase-foldase complex of the type II secretion system of *Acinetobacter baumannii*, Structure (2025), https://doi.org/10.1016/j.str.2024.12.022

similarity tool (EFI-EST): A web tool for generating protein sequence similarity networks. Biochim. Biophys. Acta *1854*, 1019–1037. https://doi.org/10.1016/j.bbapap.2015.04.015.

41. Venkatramanan, M., Sankar Ganesh, P., Senthil, R., Akshay, J., Veera Ravi, A., Langeswaran, K., Vadivelu, J., Nagarajan, S., Rajendran, K., and Shankar, E.M. (2020). Inhibition of *quorum sensing* and biofilm formation in *Chromobacterium violaceum* by fruit extracts of *Passiflora edulis*. ACS Omega *5*, 25605–25616. https://doi.org/10.1021/acsomega.0c02483.
42. Sharma, G., Parales, R., and Singer, M. (2018). *In silico* characterization of a novel putative aerotaxis chemosensory system in the myxobacterium, *Corallococcus coralloides*. BMC Genom. *19*, 757. https://doi.org/10.1186/s12864-018-5151-6.
43. Shi, Y., Liao, C., Dai, F., Zhang, Y., Li, C., and Liang, W. (2023). *Vibrio splendidus* Fur regulates virulence gene expression, swarming motility, and biofilm formation, affecting its pathogenicity in *Apostichopus japonicus*. Front. Vet. Sci. *10*, 1207831. https://doi.org/10.3389/fvets.2023.1207831.
44. Prasad, M., Obana, N., Lin, S.-Z., Zhao, S., Sakai, K., Blanch-Mercader, C., Prost, J., Nomura, N., Rupprecht, J.-F., Fattaccioli, J., and Utada, A.S. (2023). *Alcanivorax borkumensis* biofilms enhance oil degradation by interfacial tubulation. Science *381*, 748–753. https://doi.org/10.1126/science.adf3345.
45. Zirkle, R., Ligon, J.M., and Molnár, I. (2004). Cloning, sequence analysis and disruption of the mglA Gene involved in swarming motility of *Sorangium cellulosum* So ce26, a producer of the antifungal polyketide antibiotic Soraphen A. J. Biosci. Bioeng. *97*, 267–274.
46. Thi, M.T.T., Wibowo, D., and Rehm, B.H.A. (2020). *Pseudomonas aeruginosa* biofilms. Int. J. Mol. Sci. *21*, 8671. https://doi.org/10.3390/ijms21228671.
47. Okaro, U., Mou, S., Lenkoue, G., Williams, J.A., Bonagofski, A., Larson, P., Kumar, R., and Deshazer, D. (2022). A type IVB pilin influences twitching motility and *in vitro* adhesion to epithelial cells in *Burkholderia pseudomallei*. Microbiology *168*, 001150. https://doi.org/10.1099/mic.0.001150.
48. Corral, J., Pérez-Varela, M., Sánchez-Osuna, M., Cortés, P., Barbé, J., and Aranda, J. (2021). Importance of twitching and surface-associated motility in the virulence of *Acinetobacter baumannii*. Virulence *12*, 2201–2213. https://doi.org/10.1080/21505594.2021.1950268.
49. Hinsa-Leasure, S.M., Koid, C., Tiedje, J.M., and Schultzhaus, J.N. (2013). Biofilm formation by *Psychrobacter arcticus* and the role of a large adhesin in attachment to surfaces. Appl. Environ. Microbiol. *79*, 3967–3973. https://doi.org/10.1128/AEM.00867-13.
50. Sonnenschein, E.C., Syit, D.A., Grossart, H.P., and Ullrich, M.S. (2012). Chemotaxis of *Marinobacter adhaerens* and its impact on attachmentto the diatom *Thalassiosira weissflogii*. Appl. Environ. Microbiol. *78*, 6900–6907. https://doi.org/10.1128/AEM.01790-12.
51. Gedefie, A., Demsis, W., Ashagrie, M., Kassa, Y., Tesfaye, M., Tilahun, M., Bisetegn, H., and Sahle, Z. (2021). *Acinetobacter baumannii* biofilm formation and its role in disease pathogenesis: A review. Infect. Drug Resist. *14*, 3711–3719. https://doi.org/10.2147/IDR.S332051.
52. Kearns, D.B., Robinson, J., and Shimkets, L.J. (2001). *Pseudomonas aeruginosa* exhibits directed twitching motility up phosphatidylethanolamine gradients. J. Bacteriol. *183*, 763–767. https://doi.org/10.1128/JB.183.2.763-767.2001.
53. Yang, X. (2014). Moraxellaceae. In Encyclopedia of Food Microbiology, Second Edition (Elsevier Inc.), pp. 826–833. https://doi.org/10.1016/B978-0-12-384730-0.00441-9.
54. Rosenberg, T., Jiménez-Guerrero, I., Tamir-Ariel, D., Yarnitzky, T., and Burdman, S. (2022). The GDSL-lipolytic enzyme Lip1 is required for full virulence of the cucurbit pathogenic bacterium *Acidovorax citrulli*. Microorganisms *10*, 1016. https://doi.org/10.3390/microorganisms10051016.
55. Tielen, P., Rosenau, F., Wilhelm, S., Jaeger, K.E., Flemming, H.C., and Wingender, J. (2010). Extracellular enzymes affect biofilm formation of mucoid *Pseudomonas aeruginosa*. Microbiology (N. Y.) *156*, 2239–2252. https://doi.org/10.1099/mic.0.037036-0.
56. Viegas, A., Dollinger, P., Verma, N., Kubiak, J., Viennet, T., Seidel, C.A.M., Gohlke, H., Etzkorn, M., Kovacic, F., and Jaeger, K.E. (2020). Structural and dynamic insights revealing how lipase binding domain MD1 of *Pseudomonas aeruginosa* foldase affects lipase activation. Sci. Rep. *10*, 3578. https://doi.org/10.1038/s41598-020-60093-4.
57. Shibata, H., Kato, H., and Oda, J. (1998). Random mutagenesis on the *Pseudomonas* lipase activator protein, LipB: exploring amino acid residues required for its function. Protein Eng. *11*, 467–472.
58. Khattabi, M.E., Ockhuijsen, C., Bitter, W., Jaeger, K.-E., and Tommassen, J. (1999). Specificity of the lipase-specific foldases of Gram-negative bacteria and the role of the membrane anchor. Mol. Gen. Genet. *261*, 770–776.
59. Akbari, N., Khajeh, K., Rezaie, S., Mirdamadi, S., Shavandi, M., and Ghaemi, N. (2010). High-level expression of lipase in *Escherichia coli* and recovery of active recombinant enzyme through *in vitro* refolding. Protein Expr. Purif. *70*, 75–80. https://doi.org/10.1016/j.pep.2009.08.009.
60. Fang, F.C., Frawley, E.R., Tapscott, T., and Vázquez-Torres, A. (2016). Bacterial Stress Responses during Host Infection. Cell Host Microbe *20*, 133–143. https://doi.org/10.1016/j.chom.2016.07.009.
61. Flint, A., Butcher, J., and Stintzi, A. (2016). Stress Responses, Adaptation, and Virulence of Bacterial Pathogens During Host Gastrointestinal Colonization. Microbiol. Spectr. *4*. https://doi.org/10.1128/microbiolspec.vmbf-0007-2015.
62. Adolf, L.A., and Heilbronner, S. (2022). Nutritional Interactions between Bacterial Species Colonising the Human Nasal Cavity: Current Knowledge and Future Prospects. Metabolites *12*, 489. https://doi.org/10.3390/metabo12060489.
63. Nardini, M., Lang, D.A., Liebeton, K., Jaeger, K.E., and Dijkstra, B.W. (2000). Crystal structure of *Pseudomonas aeruginosa* lipase in the open conformation. The prototype for family I.1 of bacterial lipases. J. Biol. Chem. *275*, 31219–31225. https://doi.org/10.1074/jbc.M003903200.
64. Gendrin, C., Contreras-Martel, C., Bouillot, S., Elsen, S., Lemaire, D., Skoufias, D.A., Huber, P., Attree, I., and Dessen, A. (2012). Structural basis of cytotoxicity mediated by the Type III Secretion toxin ExoU from *Pseudomonas aeruginosa*. PLoS Pathog. *8*, e1002637. https://doi.org/10.1371/journal.ppat.1002637.
65. Lilic, M., Vujanac, M., and Stebbins, C.E. (2006). A common structural motif in the binding of virulence factors to bacterial secretion chaperones. Mol. Cell *21*, 653–664. https://doi.org/10.1016/j.molcel.2006.01.026.
66. Urusova, D.V., Kinsella, R.L., Salinas, N.D., Haurat, M.F., Feldman, M.F., and Tolia, N.H. (2019). The structure of *Acinetobacter*-secreted protease CpaA complexed with its chaperone CpaB reveals a novel mode of a T2SS chaperone-substrate interaction. J. Biol. Chem. *294*, 13344–13354. https://doi.org/10.1074/jbc.RA119.009805.
67. Quinaud, M., Plé, S., Job, V., Contreras-Martel, C., Simorre, J.-P., Attree, I., and Dessen, A. (2007). Structure of the heterotrimeric complex that regulates Type III Secretion needle formation. Proc. Natl. Acad. Sci. USA *104*, 7803–7808. https://doi.org/10.1073/pnas.0610098104.
68. Little, D. J., and Coombes, B. K. (2018). Molecular basis for CesT recognition of type III secretion effectors in enteropathogenic *Escherichia coli*. PLoS Pathogens *14*, e1007224. https://doi.org/10.1371/journal.ppat.1007224.
69. Ahmad, S., Tsang, K. K., Sachar, K., Quentin, D., Tashin, T. M., Bullen, N. P., Raunser, S., McArthur, A. G., Prehna, G., and Whitney, J. C. (2020). Structural basis for effector transmembrane domain recognition by type VI secretion system chaperones. ELife *9*, 1–29. https://doi.org/10.7554/eLife.62816.
70. Dym, O., Albeck, S., Unger, T., Jacobovitch, J., Branzburg, A., Michael, Y., Frenkiel-Krispin, D., Grayer Wolf, S., and Elbaum, M. (2008). Crystal structure of the *Agrobacterium* virulence complex VirE1-VirE2 reveals a flexible protein that can accommodate different partners. PNAS *105*, 11170–11175. https://doi.org/10.1073/pnas.080152510.
71. Bauer, T.L., Buchholz, P.C.F., and Pleiss, J. (2020). The modular structure of α/β-hydrolases. FEBS J. *287*, 1035–1053. https://doi.org/10.1111/febs.15071.

72. Khan, F.I., Lan, D., Durrani, R., Huan, W., Zhao, Z., and Wang, Y. (2017). The lid domain in lipases: Structural and functional determinant of enzymatic properties. Front. Bioeng. Biotechnol. *5*, 16. https://doi.org/10.3389/fbioe.2017.00016.

73. Yariv, B., Yariv, E., Kessel, A., Masrati, G., Chorin, A.B., Martz, E., Mayrose, I., Pupko, T., and Ben-Tal, N. (2023). Using evolutionary data to make sense of macromolecules with a "face-lifted" ConSurf. Protein Sci. *32*, e4582. https://doi.org/10.1002/pro.4582.

74. Izoré, T., Job, V., and Dessen, A. (2011). Biogenesis, regulation, and targeting of the Type III Secretion System. Structure *19*, 603–612. https://doi.org/10.1016/j.str.2011.03.015.

75. Worrall, L.J., Majewski, D.D., and Strynadka, N.C.J. (2023). Structural insights into Type III Secretion Systems of the bacterial flagellum and injectisome. Annu. Rev. Microbiol. *77*, 669–698. https://doi.org/10.1146/annurev-micro-032521.

76. Gilzer, D., Schreiner, M., and Niemann, H.H. (2022). Direct interaction of a chaperone-bound Type III Secretion substrate with the export gate. Nat. Commun. *13*, 2858. https://doi.org/10.1038/s41467-022-30487-1.

77. Green, E.R., and Mecsas, J. (2016). Bacterial Secretion Systems: An overview. Microbiol. Spectr. *4*. https://doi.org/10.1128/microbiolspec.vmbf-0012-2015.

78. Douzi, B., Ball, G., Cambillau, C., Tegoni, M., and Voulhoux, R. (2011). Deciphering the Xcp *Pseudomonas aeruginosa* Type II secretion machinery through multiple interactions with substrates. Journal of Biological Chemistry *286*, 40792–40801. https://doi.org/10.1074/jbc.M111.294843.

79. Michel-Souzy, S., Douzi, B., Cadoret, F., Raynaud, C., Quinton, L., Ball, G., and Voulhoux, R. (2018). Direct interactions between the secreted effector and the T2SS components GspL and GspM reveal a new effector-sensing step during Type 2 Secretion. Journal of Biological Chemistry *293*, 19441–19450. https://doi.org/10.1074/jbc.RA117.001127.

80. Korman, T.P., and Bowie, J.U. (2012). Crystal Structure of Proteus mirabilis Lipase, a Novel Lipase from the Proteus/Psychrophilic Subfamily of Lipase Family I.1. PLoS One *7*, e52890. https://doi.org/10.1371/journal.pone.0052890.

81. Karnard, D. R., Mhaisekar, D. G., and Moralwar, K. V. (1990). Respiratory mucus pH in tracheostomized intensive care unit patients: Effects of colonization and pneumonia. Critical Care Medicine *18*, 699–701.

82. Delpiano, L., Rodenburg, L.W., Burke, M., Nelson, G., Amatngalim, G.D., Beekman, J.M., and Gray, M.A. (2023). Dynamic regulation of airway surface liquid pH by TMEM16A and SLC26A4 in cystic fibrosis nasal epithelia with rare mutations. Proc. Natl. Acad. Sci. USA *120*, e2307551120. https://doi.org/10.1073/pnas.2307551120.

83. Li, T., Luo, D., Ning, N., Liu, X., Chen, F., Zhang, L., Bao, C., Li, Z., Li, D., Gu, H., et al. (2023). *Acinetobacter baumannii* adaptation to the host pH microenvironment is mediated by allelic variation in a single residue of BauA protein. PNAS Nexus *2*, pgad079. https://doi.org/10.1093/pnasnexus/pgad079.

84. Oberg, N., Zallot, R., and Gerlt, J.A. (2023). EFI-EST, EFI-GNT, and EFI-CGFP: Enzyme Function Initiative (EFI) Web Resource for Genomic Enzymology Tools. J. Mol. Biol. *435*, 168018. https://doi.org/10.1016/j.jmb.2023.168018.

85. Shannon, P., Markiel, A., Ozier, O., Baliga, N.S., Wang, J.T., Ramage, D., Amin, N., Schwikowski, B., and Ideker, T. (2003). Cytoscape: A software Environment for integrated models of biomolecular interaction networks. Genome Res. *13*, 2498–2504. https://doi.org/10.1101/gr.1239303.

86. Notredame, C., Higgins, D.G., and Heringa, J. (2000). T-coffee: A novel method for fast and accurate multiple sequence alignment. J. Mol. Biol. *302*, 205–217. https://doi.org/10.1006/jmbi.2000.4042.

87. Robert, X., and Gouet, P. (2014). Deciphering key features in protein structures with the new ENDscript server. Nucleic Acids Res. *42*, W320–W324. https://doi.org/10.1093/nar/gku316.

88. Kabsch, W. (2010). XDS. Acta Crystallogr. D Biol. Crystallogr. *66*, 125–132. https://doi.org/10.1107/S0907444909047337.

89. Arvai, A. (2013). *ADXV*. A program to display X-ray diffraction images. https://www.scripps.edu/tainer/arvai/adxv.html.

90. Brehm, W., Triviño, J., Krahn, J.M., Usón, I., and Diederichs, K. (2023). *XDSGUI*: a graphical user interface for *XDS, SHELX* and *ARCIMBOLDO*. J. Appl. Crystallogr. *56*, 1585–1594. https://doi.org/10.1107/S1600576723007057.

91. Tickle, I.J. (2007). Experimental determination of optimal root-mean-square deviations of macromolecular bond lengths and angles from their restrained ideal values. Acta Crystallogr. D Biol. Crystallogr. *63*, 1274–1283. https://doi.org/10.1107/S0907444907050196.

92. Agirre, J., Atanasova, M., Bagdonas, H., Ballard, C.B., Baslé, A., Beilsten-Edmands, J., Borges, R.J., Brown, D.G., Burgos-Mármol, J.J., Berrisford, J.M., et al. (2023). The CCP4 suite: integrative software for macromolecular crystallography. Acta Crystallogr. D Struct. Biol. *79*, 449–461. https://doi.org/10.1107/S2059798323003595.

93. McCoy, A.J. (2007). Solving structures of protein complexes by molecular replacement with Phaser. Acta Crystallogr. D Biol. Crystallogr. *63*, 32–41. https://doi.org/10.1107/S0907444906045975.

94. Mirdita, M., Schütze, K., Moriwaki, Y., Heo, L., Ovchinnikov, S., and Steinegger, M. (2022). ColabFold: making protein folding accessible to all. Nat. Methods *19*, 679–682. https://doi.org/10.1038/s41592-022-01488-1.

95. Emsley, P., and Cowtan, K. (2004). *Coot*: model-building tools for molecular graphics. Acta Crystallogr. D Biol. Crystallogr. *60*, 2126–2132. https://doi.org/10.1107/S0907444904019158.

96. Murshudov, G.N., Skubák, P., Lebedev, A.A., Pannu, N.S., Steiner, R.A., Nicholls, R.A., Winn, M.D., Long, F., and Vagin, A.A. (2011). REFMAC5 for the refinement of macromolecular crystal structures. Acta Crystallogr. D Biol. Crystallogr. *67*, 355–367. https://doi.org/10.1107/S0907444911001314.

97. Williams, C.J., Headd, J.J., Moriarty, N.W., Prisant, M.G., Videau, L.L., Deis, L.N., Verma, V., Keedy, D.A., Hintze, B.J., Chen, V.B., et al. (2018). MolProbity: More and better reference data for improved all-atom structure validation. Protein Sci. *27*, 293–315. https://doi.org/10.1002/pro.3330.

98. Laskowski, R.A., MacArthur, M.W., Moss, D.S., and Thornton, J.M. (1993). PROCHECK: a program to check the stereochemical quality of protein structures. J. Appl. Crystallogr. *26*, 283–291. https://doi.org/10.1107/S0021889892009944.

99. Joosten, R.P., Long, F., Murshudov, G.N., and Perrakis, A. (2014). The PDB_REDO server for macromolecular structure model optimization. IUCrJ *1*, 213–220. https://doi.org/10.1107/S2052252514009324.

100. Pettersen, E.F., Goddard, T.D., Huang, C.C., Couch, G.S., Greenblatt, D.M., Meng, E.C., and Ferrin, T.E. (2004). UCSF Chimera - A visualization system for exploratory research and analysis. J. Comput. Chem. *25*, 1605–1612. https://doi.org/10.1002/jcc.20084.

101. Karplus, P.A., and Diederichs, K. (2015). Assessing and maximizing data quality in macromolecular crystallography. Curr. Opin. Struct. Biol. *34*, 60–68. https://doi.org/10.1016/j.sbi.2015.07.003.

102. Emsley, P., Lohkamp, B., Scott, W.G., and Cowtan, K. (2010). Features and development of *Coot*. Acta Crystallogr. D Biol. Crystallogr. *66*, 486–501. https://doi.org/10.1107/S0907444910007493.

103. Brünger, A.T. (1997). Free R value: Cross-validation in crystallography. In Methods in Enzymology (Academic Press), pp. 366–396. https://doi.org/10.1016/S0076-6879(97)77021-6.

104. Brünger, A.T. (1992). Free R value: a novel statistical quantity for assessing the accuracy of crystal structures. Nature *355*, 472–475. https://doi.org/10.1038/355472a0.

105. Holton, J.M., Classen, S., Frankel, K.A., and Tainer, J.A. (2014). The R-factor gap in macromolecular crystallography: an untapped potential for insights on accurate structures. FEBS J. *281*, 4046–4060. https://doi.org/10.1111/febs.12922.

Please cite this article in press as: de Oliveira Silva et al., Architecture of an embracing lipase-foldase complex of the type II secretion system of *Acinetobacter baumannii*, Structure (2025), https://doi.org/10.1016/j.str.2024.12.022

CellPress

STAR★METHODS

KEY RESOURCES TABLE

REAGENT or RESOURCE	SOURCE	IDENTIFIER
Bacterial and virus strains		
Escherichia coli DH5α	Invitrogen	18265017
Escherichia coli BL21(DE3) Star	Invitrogen	C601003
Chemicals, peptides, and recombinant proteins		
para-Nitrophenyl-butyrate	Sigma-Aldrich	Cat#N9876
para-Nitrophenyl-acetate	Sigma-Aldrich	Cat#N8130
para-Nitrophenyl-caprylate	Sigma-Aldrich	Cat# 21742
para-Nitrophenyl-decanoate	Sigma-Aldrich	Cat#N0252
para-Nitrophenyl-laurate	Sigma-Aldrich	Cat#61716
para-Nitrophenyl-palmitate	Sigma-Aldrich	Cat#N2752
Critical commercial assays		
CloneJET PCR Cloning Kit	Thermo Scientific	Cat#K1231
Deposited data		
A. baumannii LipA-LipB structure	This paper	PDB: 9G8U
Oligonucleotides		
LipA_N25_F (AAAGGATCCAATG CCGAGCAAGTCAAAAGC) (Exxtend)	This paper	N/A
LipA_R (AAAGTCGACTTATAATCCTTG AAGTTTTAAACGGTTAGCGTGTTG) (Exxtend)	This paper	N/A
LipB29 Forward primer (AAACATATG TGGAGCCACCCGCAGTTCGAAAAGG GAAGCCCAGACTCGGAAAATAC TTCACCTCAG) (Exxtend)	This paper	N/A
LipB29 Reverse primer (AAACTCGAGCT AGTAGTTAAAGGGTAGTTCACCTCCTTGG) (Exxtend)	This paper	N/A
LipB52 Forward primer (TCCCTTTT CGAACTGCGG) (Exxtend)	This paper	N/A
LipB52 Reverse primer (ACTTTAAATTCA CCATTAAACGAAAATAC) (Exxtend)	This paper	N/A
Recombinant DNA		
pACYC-6xHis-YFP-LipA (For expression of LipA)	This paper	N/A
pET28b-Strep-LipB29 (For expression of $LipB_{29}$)	This paper	N/A
pET28b-Strep-LipB52 (For expression of $LipB_{52}$)	This paper	N/A
Software and algorithms		
OMNISEC Software	Malvern Panalytical	N/A
Origin 8.1 software (OriginLab)	OriginLab	https://www.originlab.com
Enzyme Function Initiative – Enzyme Similarity Tool	Oberg et al.[84]	https://efi.igb.illinois.edu/efi-est/
Cytoscape	Shannon et al.[85]	https://cytoscape.org
EXPRESSO	Notredame et al.[86]	https://tcoffee.crg.eu
ESPript	Robert and Gouet[87]	https://espript.ibcp.fr/ESPript/ESPript/
Consurf	Yariv et al.[73]	https://consurf.tau.ac.il/consurf_index.php
XDS	Kabsch[88]	https://xds.mr.mpg.de
ADXV	Arvai[89]	https://www.scripps.edu/tainer/arvai/adxv.html
XDSGUI	Brehm et al.[90]	https://xds.mr.mpg.de
STARANISO	Tickle[91]	https://staraniso.globalphasing.org/cgi-bin/staraniso.cgi

(*Continued on next page*)

Please cite this article in press as: de Oliveira Silva et al., Architecture of an embracing lipase-foldase complex of the type II secretion system of *Acinetobacter baumannii*, Structure (2025), https://doi.org/10.1016/j.str.2024.12.022

Continued

REAGENT or RESOURCE	SOURCE	IDENTIFIER
CCP4 program suite	Agirre et al.[92]	https://www.ccp4.ac.uk
PHASER	McCoy[93]	https://www.ccp4.ac.uk
AlphaFold2 ColabFold	Mirdita et al.[94]	https://github.com/sokrypton/ColabFold
COOT	Emsley and Cowtan[95]	https://www2.mrc-lmb.cam.ac.uk/personal/pemsley/coot/
REFMAC	Murshudov et al.[96]	https://www2.mrc-lmb.cam.ac.uk/groups/murshudov/content/refmac/refmac.html
MOLPROBITY	Williams et al.[97]	http://molprobity.biochem.duke.edu
PROCHECK	Laskowski et al.[98]	https://www.ebi.ac.uk/thornton-srv/software/PROCHECK/
PDB-REDO	Joosten et al.[99]	https://pdb-redo.eu
UCSF Chimera	Pettersen et al.[100]	https://www.cgl.ucsf.edu/chimera/

EXPERIMENTAL MODEL AND STUDY PARTICIPANT DETAILS

Escherichia coli DH5α cells were used in the cloning, mutagenesis, and large-scale plasmid production procedures. *E. coli* BL21 Star (DE3) cells were used for recombinant protein expression.

METHOD DETAILS

Construct design

All genes were amplified from the genomic DNA of *A. baumannii* DSM 30011. The region of *lipA* corresponding to the soluble domain of LipA without a signal peptide (residues 25-324) was amplified using primers LipA_N25_F (5'-AAAGGATCCAATGCCGAGCAAGTC AAAAGC-3') and LipA_R (5'-AAAGTCGACTTATAATCCTTGAAGTTTTAAACGGTTAGCGTGTTG-3') and cloned into vector pJET 1.2 (CloneJET PCR Cloning Kit, Thermo Scientific™). The product was subcloned into a modified pACYC vector, containing sequences for a 6xHis-tag and the monomeric yellow fluorescent protein (mCitrine) followed by a Tobacco Etch Virus (TEV) protease cleavage site, using *BamHI* and *SalI* restriction sites. $LipB_{29}$ was generated by amplifying the region of *lipB* corresponding to the soluble domain of LipB without a signal peptide or a transmembrane helix (residues 29-343) using primers (5'- AAACATATGTGGAGCCACCC GCAGTTCGAAAAGGGAAGCCCAGACTCGGAAAATACTTCACCTCAG-3') and (5'- AAACTCGAGCTAGTAGTTAAAGGGTAGTTCA CCTCCTTGG-3'), which include the coding sequence for an N-terminal Strep-tag, and cloned into pJET 1.2. The gene was subsequently subcloned into pET30b using *NdeI* and *XhoI*. Subsequently, based on our limited proteolysis analysis, a shorter proteolysis-resistant version of LipB ($LipB_{52}$, residues 52-343) was generated by PCR-based mutagenesis using primers (5'- TCCCTTTTCG AACTGCGG-3') and (5'- ACTTTAAATTCACCATTAAACGAAAATAC-3'). NCBI accession numbers for LipA and LipB are Genbank: PNH16507.1 and Genbank: PNH16508.1, respectively.

Protein expression, purification and crystallization

Vectors encoding LipA and $LipB_{52}$ were co-transformed into *E. coli* BL21 Star (DE3) cells and grown at 37°C and 200 rpm in TB medium supplemented with kanamycin at 100 μg/ml and chloramphenicol at 34 μg/mL. When the absorbance at 600 nm reached 0.6 A.U., protein expression was induced by adding 0.5 mM isopropyl β-D-1-thiogalactopyranoside (IPTG). Cultures were grown for 16 h at 20°C and 200 rpm, and harvested by centrifugation at 10,000 x g for 30 min at 4°C. The cell pellet was resuspended in lysis buffer [50 mM Tris-HCl (pH 8.0), 200 mM NaCl, 5 mM $CaCl_2$ supplemented with 1mM phenylmethylsulfonyl fluoride (PMSF), 0.1 mg/mL lysozyme and 5 U/mL benzonase], then sonicated on ice. The cell lysate was centrifuged at 15,000 x g for 1 hour at 4°C. The supernatant was loaded onto a nickel–nitrilotriacetic acid (Ni-NTA) column pre-equilibrated in buffer A [50 mM Tris-HCl (pH 8.0), 200 mM NaCl, 5 mM $CaCl_2$], then a two-step wash was performed using buffer A followed by buffer B [50 mM Tris-HCl (pH 8.0), 200 mM NaCl, 5 mM $CaCl_2$, 35 mM Imidazole]. The sample was eluted in buffer containing 50 mM Tris-HCl (pH 8.0), 200 mM NaCl, 5 mM $CaCl_2$, and 100 mM Imidazole. Imidazole was removed from the sample by discontinuous diafiltration. The 6xHis + YFP tag was removed from LipA by incubating the sample overnight at 4°C with 1:15 (m/m) TEV protease, followed by a 2-hour incubation at room temperature. For separation of the cleaved protein, the sample was loaded onto a Ni-NTA column pre-equilibrated in buffer A. The flow-through was loaded onto a HiLoad 16/600 Superdex 200 column (Cytiva) equilibrated in buffer A.

Crystals were obtained by vapor diffusion using the hanging drop method and a sample at 7 mg/mL. Initial poorly diffracting LipA-LipB crystals were obtained in 1.5 M ammonium sulfate and 0.1 M Bis-Tris propane (pH 7.5). Crystals were improved using the micro-seeding technique in 1.5 M ammonium sulfate, 0.1 M Bis-Tris propane (pH 7.5) and 5% polyethylene glycol (PEG) 400.

Limited proteolysis

Pure LipA-LipB$_{29}$ samples were incubated with either trypsin, chymotrypsin or papain in a 1:200 (m/m) ratio at 37°C for 24h. Samples were collected at different time points, and reactions were stopped by the addition of protein loading dye containing 10% SDS and by heating samples at 95°C for 5 minutes, followed by freezing at -20°C. The extent of proteolysis was verified by running samples on a polyacrylamide gel.

Light Scattering

The oligomeric state of the purified LipA-LipB complex was determined in a SEC-RALS/LALS (Size Exclusion Chromatography coupled to Right Angle Light Scattering and Low Angle Light Scattering) experiment. Two different oligomeric states of the complex could be isolated from a preparative size exclusion chromatography column (HiLoad Superdex 200 16/600, Cytiva) in buffer A. Samples were treated separately, concentrated to 1 mg/mL and injected onto a Superdex 200 10/300 GL (Cytiva) column in buffer A at 0.3 mL/min, using an OmniSEC system (Malvern Panalytical). Molecular weights and hydrodynamic radii were calculated by the OMNISEC Software. Experiments were performed in triplicate.

Biochemical characterization

The catalytic performance of LipA-LipB was assessed using a 96-well plate format with a reaction volume of 100 μL. Each reaction contained 1 mM para-nitrophenyl-butyrate (pNPB) in a 40 mM sodium phosphate buffer (pH 6.5). Reactions were conducted at 30°C for 10 minutes using a Veriti Thermal Cycler (Applied Biosystems, Thermo Fisher Scientific) and terminated by adding 100 μL of pure acetonitrile (Sigma-Aldrich). Enzymatic hydrolysis was monitored by the release of para-nitrophenyl (pNP) at 405 nm using an Infinite®200 PRO microplate spectrophotometer reader (TECAN). All experiments were performed in triplicate, and nonenzymatic hydrolysis effects were subtracted from the measurements. Results were expressed as relative activity (%), normalized against the maximum catalytic activity observed in each experiment. The optimum temperature was evaluated using a range from 30°C to 60°C, while optimum pH was assessed from pH 4.0 to 7.5 using sodium citrate (pH 4.5 to 6.0) and sodium phosphate (pH 6.5 to 7.5) buffers, each at a final concentration of 40 mM, at 40°C.

Substrate specificity was examined using various para-nitrophenyl (pNP) esters containing variable acyl chain lengths, namely pNP acetate (C2:0; CAS Number 830-03-5), pNP butyrate (C4:0; CAS Number 2635-84-9), pNP caprylate (C8:0; CAS Number 1956-10-1), pNP decanoate (C10:0; CAS Number 1956-09-8), pNP laurate (C12:0; CAS Number 1956-11-2), and pNP palmitate (C16:0; CAS Number 1492-30-4). All pNPs esters were purchased from Sigma-Aldrich® and prepared at a stock concentration of 50 mM. Enzyme activity was determined in a reaction containing 1 mM of each p-nitrophenyl reagent (C2 to C16) buffered with 40 mM sodium phosphate buffer pH 6.5 at 40°C.

Regarding enzyme kinetics, the apparent Michaelis-Menten parameters (K_m and K_{cat}) were determined under optimal pH and temperature conditions using pNPB as a substrate. Data analysis was performed using Origin 8.1 software (OriginLab) through nonlinear regression of the Michaelis-Menten plot.

Sequence analyses

Sequence similarity networks were generated by submitting the full-length sequence of LipB from *A. baumannii* DSM30011 to EFI-EST (Enzyme Function Initiative – Enzyme Similarity Tool)[84] using the UniRef90 database and excluding fragments. An alignment score cutoff of 35 was selected and SSNs were imported into Cytoscape.[85] An identity cutoff of 45% was used to separate clusters, and clusters with more than 15 sequences were selected for further analyses. Consensus sequences for the conserved Lif motifs were generated by multiple sequence analyses of all sequences in each cluster using the EXPRESSO algorithm on the T-COFFEE server.[86] Alignment images were generated using ESPript (https://espript.ibcp.fr).[87]

To compare clusters, representative sequences were selected by aligning all sequences in each cluster using the Uniprot Align tool and selecting the centroid sequence, except when a Swiss-Prot curated sequence was available, in which case this was the sequence used. Lipases encoded by genes adjacent to each selected foldase gene were chosen as the representative sequences. Multiple sequence alignments of representative sequences were generated and submitted to Consurf[73] for conservation analyses, and sequences with Consurf scores of 7 or higher were considered ''Highly conserved''.

Data collection, structure determination and refinement

Crystals were flash cooled in liquid nitrogen in a solution composed of the crystallization conditions supplemented with 30 % PEG 400. X-ray diffraction data were collected under a nitrogen stream at 100 K on the MANACÁ beamline of Sirius, LNLS, Brazil (Table 1). Data were collected to 3.17 Å. X-ray diffraction images were indexed and scaled with XDS.[88] ADXV[89] and XDSGUI[90] were used to perform data quality and resolution cutoff check-ups.[101] The maximum possible resolution was determined using STARANISO.[91] The reduced X-ray diffraction data was imported into the CCP4 program suite.[92] The LipA-LipB structure was solved by molecular replacement using PHASER[93] and an AlphaFold2 ColabFold[94]-generated model. The structure was completed by cycles of manual model building with COOT.[95] Water molecules were added to the residual electron density map as implemented in COOT.[102] Crystallographic macromolecular refinement was performed with REFMAC.[96] Cycles of model building and refinement were performed until R_{work} and R_{free} converged.[103–105] The stereochemical quality of the refined models was verified with MOLPROBITY,[97] PROCHECK[98] and PDB-REDO.[99] Figures displaying protein structures were generated with UCSF Chimera.[100] A stereo depiction

Please cite this article in press as: de Oliveira Silva et al., Architecture of an embracing lipase-foldase complex of the type II secretion system of *Acinetobacter baumannii*, Structure (2025), https://doi.org/10.1016/j.str.2024.12.022

of a representative part of the electron density map is shown in Figure S6. Final refined model coordinates and structure factors were deposited in the Protein Data Bank (PDB, http://www.rcsb.org), ID code: 9G8U.

QUANTIFICATION AND STATISTICAL ANALYSIS

SEC-RALS/LALS experiments were performed in triplicate. Molecular weight and hydrodynamic radii calculations and statistical analysis were performed using the OmniSEC software as instructed by the equipment manufacturer.

Biochemical assays were also performed in triplicate. Mean and standard deviation were calculated using GraphPad Prism (GraphPad). Data analysis for enzyme kinetics was performed using Origin 8.1 software (OriginLab) through nonlinear regression of the Michaelis-Menten plot.

X-ray diffraction data was processed as described in the Method section. Statistical information related to data processing, refinement, and validation is shown in Table 1.